1 ***Title***

2 Local reciprocal release of GABA from dendritic spines of olfactory bulb granule cells

3 requires local sodium channel activation and occurs on both fast and slow timescales

4 ***Authors***

5 Vanessa Lage-Rupprecht[1], Tiffany Ona-Jodar[1,2], Gagik Yeghiazaryan[1], Balázs Rózsa[3] &

6 Veronica Egger[1]

7 ***Affiliations***

8 1. Neurophysiology, Institute of Zoology, Universität Regensburg, 93040 Regensburg,

9 Germany; 2. Institut D'Investigacions Biomèdiques, 08036 Barcelona, Spain; 3. Two-Photon

10 Imaging Center, Institute of Experimental Medicine, Hungarian Academy of Sciences, 1039

11 Budapest, Hungary.

12 ***Abstract***

13 In the rodent olfactory bulb the smooth dendrites of the principal glutamatergic mitral cells
14 (MCs) engage in reciprocal dendrodendritic interactions with the large spines of GABAergic
15 granule cells (GC), giving rise to local postsynaptic activation of voltage-gated Na^+ channels
16 (Na_v) within the spines. It is not known yet whether individual MC inputs can also trigger the
17 reciprocal release machinery. Here we show that local activation via two-photon uncaging of
18 glutamate causes GC spines to release GABA both synchronously and asynchronously onto
19 MC dendrites, detected as uncaging-evoked reciprocal IPSCs at the MC soma. This local
20 recurrent inhibition requires GC Na_v activation, indicating that individual spine spikes can
21 induce release from the reciprocal spine. Interestingly, NMDA receptors also play a major,
22 probably cooperative, role for GABA release. Finally, we demonstrate prolonged postsynaptic
23 elevations of both $[Ca^{2+}]_i$ and $[Na^+]_i$ within the GC spine head, on the same time scale as
24 asynchronous release.

25 ***Introduction***

26 Reciprocal dendrodendritic microcircuits can be found in several areas of the nervous system
27 and are especially abundant in the vertebrate olfactory bulb (Crespo et al., 2013), where the
28 dendrites of the principal mitral and tufted cells (MTCs) engage in reciprocal dendrodendritic
29 interactions with at least three major subtypes of local GABAergic neurons, namely
30 periglomerular cells in the glomerular layer, and parvalbumin and granule cells (GC) in the
31 external plexiform layer. What sets the latter synapse apart from the other bulbar reciprocal
32 arrangements is its location within a large spine on the GC side. These spines feature
33 particularly long necks (Woolf et al., 1991) which might serve to electrically isolate the
34 synapse and boost local processing (e.g. Miller et al., 1985; Spruston, 2008). Indeed, we have
35 gathered evidence that postsynaptic potentials in GC spines are electrically
36 compartmentalized and thus can locally activate voltage-gated Na_v channels which in turn
37 activate classical presynaptic N/P/Q Ca^{2+} channels within the spine (Bywalez et al., 2015).
38 These observations enhance our earlier notion of the reciprocal spine as a mini-neuron that
39 can generate synaptic output on its own (Egger and Urban, 2006).

40 While there have been many earlier studies of recurrent dendrodendritic inhibition at the MC-
41 GC synapse, so far it is an open question whether a unitary, purely local activation of the
42 spine's microcircuit can indeed trigger release of GABA back onto the exciting mitral cell.
43 The issue is still unresolved because the earlier studies are based on the application of a strong
44 stimulus to a voltage-clamped mitral cell (MC), namely a depolarization to 0 mV for mostly
45 20-50 ms (Isaacson and Strowbridge, 1998; Schoppa et al., 1998; Halabisky et al., 2000;
46 Isaacson, 2001; Chen et al., 2000). This protocol - called MC-step in the following - is likely
47 to cause a substantial release of glutamate from the lateral MC dendrites and was also shown
48 to invoke glutamate spillover between MC lateral dendrites (Isaacson, 1999). MC-step was
49 found to result in long-lasting recurrent inhibition with both synchronous and asynchronous
50 components, the latter with a time constant of ~ 500 ms. For this recurrent inhibition, NMDA

51 receptor (NMDAR) activation was shown to be an important source of Ca^{2+} entry that triggers
52 release of GABA from the GC spine, especially under conditions of zero extracellular
53 $[Mg^{2+}]_e$. NMDARs are known to substantially contribute to synaptic transmission at this
54 synapse (Isaacson and Strowbridge, 1998; Schoppa et al., 1998) and to postsynaptic Ca^{2+}
55 entry, also at normal $[Mg^{2+}]_e$ (Egger et al., 2005). Other mechanimss involved in recurrent
56 release following MC-step include high-voltage activated Ca^{2+} channels (HVACCs),
57 AMPARs under conditions of reduced desensitization (both Isaacson, 2001), and TRPC1/4-
58 mediated signalling pathways downstream of the NMDAR (Stroh et al., 2012).
59 The substantial asynchronous component following MC-step is likely to originate within the
60 GC, since MC-step caused prolonged activation of GCs (Schoppa et al., 1998) and
61 asynchronous responses were demonstrated following flash photolysis of Ca^{2+} in MC lateral
62 dendrites (Chen et al., 2000).
63 As to the MC side, MC lateral dendrites are known to be densely covered with GABAergic
64 synapses (Bartel et al., 2015; Sailor et al., 2016). These inputs become strongly attenuated
65 with distance from the MC soma ($\lambda \sim 80$ µm, Lowe, 2002) but are probably capable of
66 shunting propagating APs at any point along the dendrite as shown by GABA application or
67 electrical stimulation of GCs (Lowe, 2002; Xiong et al., 2002). Many of these GABAergic
68 synapses are reciprocal spine inputs from GCs, especially close to the MC soma. Recent
69 studies have revealed substantial reciprocal dendrodendritic interactions also with other
70 GABAergic cell types such as SOM+ neurons, CRH+ neurons and PV+ neurons (populations
71 in part overlap; Toida et al., 1994; Lepousez et al., 2010; Huang et al., 2013; Kato et al.,
72 2013; Miyamichi et al., 2013). To our current knowledge these other neuron types do not bear
73 spines but feature smooth dendrites.
74 Aside from postsynaptic $GABA_A$Rs, MC lateral dendrites are known to bear scattered NMDA
75 autoreceptors (Sassoe-Pognetto et al., 2003), and AMPA autoreceptors have been detected in
76 the apical tuft and at the soma, giving rise to both autoexcitation and spillover effects

77 (Aroniadou-Anderjaska et al., 1999; Isaacson, 1999; Friedman and Strowbridge, 2000; Didier
78 et al., 2001; Salin et al., 2001). Lateral excitation between MCs via this pathway appears to
79 happen mostly in the tuft (e.g. Pimentel and Margrie, 2008). MC NMDA autoreceptors do not
80 contribute to basal synaptic transmission between MCs and GCs (Egger, 2008).
81 Here we aim to determine whether – and possibly how - single inputs from MC lateral
82 dendrites to GC spines can also trigger recurrent release of GABA from the reciprocal
83 synapse, using recordings from labeled MCs and two-photon uncaging (TPU) of glutamate
84 along their lateral dendrite near Venus-tagged GC spines.
85
86 ***Results***
87 *Experimental configuration*
88 To enable pharmacological interference with components of the reciprocal microcircuit such
89 as Na_Vs and HVACCs, we bypassed release from the MC presynapse via TPU of DNI-caged
90 glutamate (DNI; Chiovini et al., 2014; Bywalez et al., 2015) in acute juvenile rat olfactory
91 bulb slices, in combination with somatic whole-cell voltage-clamp recordings from MCs. To
92 visualize the lateral dendrites, MCs were filled with the dye Alexa594 (50 μM). Fig. 1A
93 shows a schematic and example image of the recording configuration in a brain slice from a
94 VGAT-Venus animal.
95 In all MC recordings we observed a high basal frequency of spontaneous events (4.5 ± 2.1
96 Hz, n = 14). High spontaneous activity levels are a general hallmark of the olfactory bulb
97 network and also observed in GCs (Egger and Urban, 2006). Wash-in of 1 mM DNI further
98 increased this high basal frequency by on average 1.87 ± 1.21 times control ($P < 0.01$, Fig.
99 1B); this effect can be explained by the disinhibition resulting from a partial blockade of
100 $GABA_A$Rs by DNI. Since ~ 80% of the neurons of the olfactory bulb are inhibitory (e.g.
101 Shepherd and Greer, 2004), even partial disinhibition is likely to yield strong increases in
102 overall activity. DNI reduced the mean spontaneous IPSC amplitude to a fraction of 0.47 ±

103 0.16 (control amplitude: 47 ± 17 pA, n = 14, P < 0.001, Fig. 1B and S1B1). In the presence of
104 DNI, spontaneous IPSCs had a mean rise time τ_{rise} = 7.4 ± 2.5 ms and decayed with a half-
105 duration $\tau_{1/2}$ = 30.8 ± 9.5 ms (n = 14 mitral cells). The $GABA_AR$ antagonist Bicuculline
106 (BCC, 50 µM) blocked spontaneous activity almost completely (frequency: 0.13 ± 0.10 of
107 control, n = 6, Fig. 1B, S1B2).
108 Thus the detectability of TPU-evoked reciprocal release of GABA is lowered by both the
109 amplitude reduction and the increase in spontaneous activity caused by 1 mM DNI.
110 Therefore, we also tested RuBi glutamate (500 µM) which has been reported to exert
111 considerably less of a blocking effect on GABAergic transmission than MNI glutamate (Fino
112 et al., 2009). However we could not reliably replicate the GC spine signal $(\Delta F/F)_{TPU}$ and the
113 GC uEPSPs compared to the signals obtained with both DNI and MNI (tested in n = 10
114 spines, see also Table S2 in Bywalez et al., 2015). Therefore all further experiments were
115 performed with 1 mM DNI.
116 Since in initial experiments we found evidence for activation of both NMDA and AMPA
117 autoreceptors on MC dendrites at a holding potential of -70 mV, MCs were clamped to 10
118 mV, near the reversal potential of ionotropic glutamate receptors (Isaacson, 1999; Friedman
119 and Strowbridge, 2000), in later experiments. Throughout all experiments we used
120 physiological levels of $[Mg^{2+}]_e$ (1 mM), to not overestimate the NMDAR contribution to
121 recurrent inhibition; previous experiments have shown that GC spine NMDARs are activated
122 during small EPSPs in the presence of 1 mM $[Mg^{2+}]_e$ and contribute ~50 % to the total
123 postsynaptic Ca^{2+} signal $(\Delta F/F)_{syn}$ (Egger et al., 2005).
124 *Triggering of reciprocal IPSCs via TPU is possible*
125 To prevent overstimulation with glutamate, we uncaged with similar laser parameters as in the
126 previous study (Bywalez et al., 2015), in which TPU-evoked GC signals were
127 indistinguishable from unitary spontaneous events. Uncaging was performed either 'blindly'

128 at several spots along the dendrite (e.g. Fig. 2B) in WT rats or in the immediate vicinity of
129 GC spines that were visible in VGAT-Venus rats and in close proximity (0.2 – 0.5 µm) to the
130 mitral cell lateral dendrite (e.g. Fig. 1A, Fig. 2A). Responses were detectable in 53 out of 166
131 uncaging experiments (see Methods). In both stimulation paradigms uncaging was performed
132 at distances < 40 µm from the MC soma (mean distance of uncaging spots with responses 18
133 ± 8 µm, n = 27, Fig. S1A1). The rationale for this choice was twofold. First we aimed to
134 minimize electrotonic attenuation of IPSCs, since IPSC amplitudes were already diminished
135 by the caged compound (see above, Fig. 1B and S1B1) and IPSCs from more distal locations
136 are of neglibible impact at the MC soma (e.g. McIntyre and Cleland, 2016). Second, this
137 strategy is likely to preferentially stimulate GC spines rather than PV+ neuron dendrites, since
138 the GC inputs are located more proximally as compared to the widely distributed PV+ neuron
139 inputs (Kato et al., 2013; Miyamichi et al., 2013). In addition, PV+ neuron dendrites are
140 smooth and thus in the experiments in VGAT-Venus rats with visible GC spines an accidental
141 activation of PV neurons is yet less likely to occur.
142 TPU of glutamate resulted in consecutive triggered responses and failures in MCs (Fig. 1D
143 left). Responses were classified as triggered if they were observed repeatedly within the same
144 time window (see Methods). Next we tested whether these triggered responses were indeed
145 GABAergic by applying the $GABA_AR$ antagonist Bicuculline (50 µM), which invariably
146 blocked responses completely (Fig. S1C1, n = 7, P < 0.01, Wilcoxon test). Thus in the
147 following the triggered events are denoted as urIPSCs (**u**ncaging-evoked **r**eciprocal IPSCs).
148 To establish the stability of urIPSCs, we performed TPU over an extended period of time at
149 0.033 Hz and measured the mean amplitude of responses during the first and last 5-10
150 photostimulations (with at least 10 min in between to mimick the time course of
151 pharmacological manipulations, Fig. 1C). There was no significant difference (n = 7, ratio last
152 to first 0.95 ± 0.15, P = 0.74).

153 The amplitude of triggered urIPSCs was on average 12 ± 8 pA (Fig. 1E, n = 32), with a rise
154 time of 6 ± 3 ms (in n = 25 MCs clamped to +10 mV). There was no detectable correlation
155 between the urIPSC amplitude and the distance from the soma, although in our data set all
156 three examples with larger amplitudes (> 25 pA) occurred in the more proximal half of the
157 covered dendritic range (n = 20, r = -0.07, Fig. S1A2).
158 The average release probability from the reciprocal spine was estimated as $P_r = 0.34 \pm 0.11$
159 (Fig. 1E, range 0.13 - 0.60, based on n = 44 MCs, see Methods). Due to the presence of DNI
160 and the ensuing difficulty of urIPSC detection this result might represent an underestimate; on
161 the other hand, connections with a very low $P_r < 0.2$ could go unnoticed, since at least two
162 responses within the same time window were required to qualify the experiment for the
163 presence of triggered urIPSCs.
164 Triggered urIPSCs were observed within a far ranging distribution, with the latency measured
165 from the onset of TPU pulse onwards (Fig. 1E). Latency values were not normally distributed,
166 with a first peak within the first 10 ms post TPU onset (n = 13), a second peak around 30 ms
167 (n = 19 within the range 10-50 ms) and three delayed events past 50 ms. An example for such
168 a late triggered response is shown in Fig. S1E1.
169 In most experiments we detected asynchronous urIPSCs following the first triggered event
170 which were quantified both via integral analysis and counting of events (Fig. 1D, see
171 Methods). Both the area and the number of events increased highly significantly in the 500
172 ms interval following TPU ('post') compared to the same interval right before ('pre'; n = 27,
173 mean increase of integral to 1.50 ± 0.55 relative to 'pre'; mean increase in event number to
174 1.25 ± 0.37 relative to 'pre'; n = 27, $P < 0.001$ for both; absolute values in 'pre' interval
175 integral 2.40 ± 1.83 pAs, events 26.1 ± 14.9 shown in Fig. S1D1). The increase in area is also
176 significant ($P < 0.003$) if the extra area provided by the first triggered response was
177 subtracted. The total duration of recurrent inhibition was on average 179 ± 137 ms (range 32
178 – 533 ms, n = 26, Fig. S1D2). These data demonstrate that asynchronous recurrent inhibition

179 also happens for unitary stimulation of a single spine. In the last part of this study we
180 investigate possible mechanisms underlying this asynchronous output (see below).
181 From all these experiments we conclude that local, unitary TPU of glutamate can indeed
182 trigger the reciprocal release of GABA, providing proof that the reciprocal microcircuit can
183 be activated by single synaptic inputs under physiological conditions (normal levels of Mg^{2+}).
184 The substantial asynchronous component indicates that delayed release does not require
185 global signals within the entire GC.
186 *Sodium channel blockade decreases urIPSCs*
187 Next, we investigated a possible contribution of Na_v activation to urIPSC generation by
188 application of 500 nM TTX. Fig. 2 illustrates that TTX substantially reduced both triggered
189 and spontaneous events. On average, urIPSC amplitudes were reduced to a fraction of 0.17 ±
190 0.34 of control (Fig. 2C, n = 12, $P < 0.005$; absolute control amplitudes for -70 mV: -7.8 ± 3.6
191 pA, for 10 mV: 15.4 ± 12.4 pA). Only one experiment did not show any effect, in line with
192 our earlier observation that there is a broad variability in the degree to which TPU-evoked GC
193 spine Ca^{2+} signals are reduced by TTX (Bywalez et al., 2015). The relative increase in area
194 post TPU compared to pre TPU (Δ area) decreased to 0.28 ± 0.21 of the relative increase in Δ
195 area in control (see Methods; control in DNI alone; n = 10, $P < 0.005$, Fig. 2D).
196 Fig. S2 shows the analysis of TTX effects on spontaneous activity, which was also strongly
197 decreased to a fraction of 0.24 ± 0.17 of control (n = 10, $P < 0.005$). The few remaining
198 events were blocked by BCC (to a fraction of 0.16 ± 0.16 of TTX, n = 10).
199 Thus Na_vs are essential to trigger GABA release from the reciprocal spines.
200 *High-voltage activated Ca^{2+} channels in the spine contribute to GABA release*
201 HVACCs have been implied to mediate recurrent release from reciprocal spines (Isaacson,
202 2001) and are activated by Na_vs, contributing a substantial fraction of 30% to the postsynaptic
203 Ca^{2+} signal in the GC spine (Bywalez et al., 2015). To directly test the hypothesis that

204 HVACC activation is required for release of GABA, we blocked N/P/Q type Ca^{2+} channels
205 with 1 μM ω-conotoxin MVIIC (CTX; Bloodgood and Sabatini, 2007; Bywalez et al., 2015).
206 Fig. 3 shows the resulting substantial decrease of urIPSCs to a fraction of 0.08 ± 0.14 of
207 control (from a mean amplitude of 11.3 ± 5.7 pA; n = 8, P < 0.005, Fig. 3C). This decrease
208 was not different from the effect of TTX on urIPSC amplitude described above (P = 0.35
209 ratios in CTX vs TTX). The relative Δ area following TPU compared to baseline decreased to
210 0.39 ± 0.23 of control (control in DNI alone; n = 9, P < 0.005, Fig. 3D), which was also not
211 significantly different from the effect of TTX on Δ area described above (P = 0.15 vs TTX).
212 The effect of CTX on spontaneous activity was less pronounced than that of TTX, as shown
213 in Fig. S3. The frequency of events decreased to a fraction of 0.53 ± 0.15 of control (n = 7
214 cells, control vs CTX: P = 0.018; CTX vs TTX: P = 0.005), and again the remaining events
215 were blocked in the presence of the $GABA_AR$ antagonist BCC (to a fraction of 0.05 ± 0.05 of
216 CTX, n = 7).
217 We conclude that HVACC activation is required for release of GABA from the reciprocal
218 spine following local input. Thus the spine indeed acts similarly to a mini-neuron that can
219 process single synaptic inputs to generate recurrent output. The local input triggers a local AP
220 and therewith Ca^{2+} entry via HVACCs which then brings about release.
221 *NMDA receptors are also relevant for recurrent release*
222 Because NMDAR activation was clearly not dependent on Na_v activation in our earlier study
223 where postsynaptic GC spine Ca^{2+} signals in the presence of TTX were substantially reduced
224 further by APV (Bywalez et al., 2015), and because the blocking effects of TTX or CTX on
225 urIPSCs were rather strong, we hypothesized that NMDAR blockade would have only mild
226 effects on fast recurrent release. Also, an earlier study of dendrodendritic inhibition under
227 conditions of normal Mg^{2+} indicated that release from GC spines is mostly triggered in the
228 classical way via HVACC activation (Isaacson, 2001). Intriguingly, however, the application
229 of 25 μM D-APV resulted in a decrease of urIPSC amplitudes to on average 0.22 ± 0.21 of

230 control (from a mean amplitude of 13.8 ± 8.6 pA, n = 10, P < 0.002, Fig. 4C). All individual
231 experiments showed the amplitude decrease, albeit with variable degree (range 0.00 - 0.68 of
232 control). There was no significant correlation between the relative amplitude decrease and the
233 urIPSC latency (r = 0.26, P = 0.23). The effect of APV on urIPSC amplitude was statistically
234 not different from the effect of TTX or CTX (P = 0.12 and P = 0.08). The relative increase in
235 Δ area following TPU compared to baseline decreased to 0.40 ± 0.28 of control (control in
236 DNI alone; n = 10, P < 0.003, Fig. 4D), which was also not different from the effect of TTX
237 or CTX on Δ area (P = 0.19 and P = 0.47).
238 In addition APV also substantially reduced spontaneous activity, to a frequency of 0.19 ± 0.08
239 of control (n = 9, P < 0.01, Fig. S4A, B). This effect of APV was similar to that of TTX (P =
240 0.84) and significantly more pronounced than that of CTX (P < 0.001). The few remaining
241 events in APV were blocked by BCC (to a fraction of 0.02 ± 0.04 of APV, n = 9, Fig. S4B).
242 Since the strong effect of NMDAR blockade on urIPSCs was surprising to us, we sought to
243 provide a second line of evidence for this finding in an experimental setting that does not
244 involve uncaging of glutamate. Recently, Nunes and Kuner (2018) clearly demonstrated that
245 the smooth and uniform negative voltage deflection following single MC APs elicited by
246 somatic current injection is not an intrinsic afterhyperpolarization. Rather, it mainly reflects
247 recurrent inhibition from a large set of reciprocal synapses since it could be strongly reduced
248 by either $GABA_AR$ blockade or ionotropic glutamate receptor blockade; therefore they
249 termed this signal rIPSP (recurrent IPSP). We used the same paradigm to test whether
250 NMDAR blockade alone could interfere with recurrent inhibition. Single MC AP rIPSPs (n =
251 11 MCs) had a mean amplitude ΔV_m = – 8.7 ± 2.3 mV and a mean half duration $\tau_{1/2}$ = 37 ± 9
252 ms, whereas the entire hyperpolarizing phase lasted for on average 382 ± 78 ms, in line with
253 asynchronous release from GC spines (compare to duration of barrages Fig. S1D2; see
254 Methods). Fig. 4E, F shows that APV application significantly reduced the mean rIPSP
255 amplitude to a fraction of 0.64 ± 0.20 of control (P < 0.005), while the rIPSP half duration

256 was decreased, but not significantly so, to a fraction of 0.91 ± 0.24 of control (P = 0.06), and
257 also the total duration of the hyperpolarization did not change significantly (fraction of
258 control 0.96 ± 0.40, P = 0.27, not shown). The remaining rIPSP was further reduced
259 substantially in BCC, to a fraction of 0.13 ± 0.19 of control (from 8.9 ± 2.9 mV, n = 4 MCs,
260 example in Fig. S4D).
261 In summary, these results imply that NMDARs do play a presynaptic role for both fast and
262 slow recurrent release of GABA from the reciprocal spine. Since the Na_v/HVACC pathway is
263 also required for GABA release, it appears likely that there is a fast cooperative mechanism
264 between NMDARs and the classical combination of Na_vs and HVACCs (see discussion).
265 *Time course of synaptic spine Ca^{2+} and Na^+ signals with minimal exogenous buffering*
266 While HVACC-mediated Ca^{2+} entry operates on a fast time scale and coupling to release is
267 fast in a substantial subset of spines (Fig. 1E), slower actions downstream of both Na_v and
268 NMDAR activation are required to trigger cascades that result in asynchronous release events.
269 A number of global mechanisms has been proposed to promote asynchronous release from
270 GC spines, including a global GC spike delay due to the prominent I_A current (Schoppa and
271 Westbrook, 1999; Kapoor and Urban, 2006) and prolonged Ca^{2+} entry due to global spiking in
272 coincidence with synaptic TRPC14 activation (Egger, 2008; Egger and Stroh, 2009; Stroh et
273 al., 2012). On the other hand, we found unitary EPSPs evoked by spontaneous MTC input or
274 local TPU to decay with a time constant < 50 ms (as recorded at the GC soma, Bywalez et al.,
275 2015). To further investigate the mechanisms underlying the asynchronous component of
276 reciprocal GABA release in the absence of a global Na^+ spike and in levels of normal Mg^{2+}
277 we aimed to detect local postsynaptic Ca^{2+} signalling in GC spines with as little exogenous
278 buffering as possible, since sluggish extrusion of Ca^{2+} might also contribute to delayed release
279 (Egger and Stroh, 2009). The low affinity dye OGB-6F ($K_d \approx 8$ µM, Tran et al., 2018) was
280 used at a concentration of 100 µM, where the kinetics of OGB-6F fluorescence transients in
281 response to single somatic action potentials $(\Delta F/F)_{sAP}$ are identical to the kinetics determined

282 by extrapolation of measurements with varying concentrations of OGB-1 ($K_d \approx 0.2$ μM) to
283 zero added buffer (Egger and Stroh, 2009). TPU of DNI with similar parameters as in
284 Bywalez et al. (2015) evoked Ca^{2+} transients $(\Delta F/F)_{TPU}$ with a mean amplitude of 24 ± 12 %
285 and a mean $\tau_{1/2}$ of 440 ± 180 ms (n = 16 spines, Figure 5 A, B). While $\tau_{1/2}$ was difficult to
286 analyse in some of the individual spine responses because of noise, the averaged transient
287 yielded a $\tau_{1/2}$ of ~ 600 ms, clearly substantially slower than the half duration of AP-mediated
288 transients recorded in a subset of these spines (n = 8, $\tau_{1/2}$ of averaged $\Delta F/F$ ~ 100 ms, Fig. 5A
289 bottom).
290 Since both Na_vs and AMPAR/NMDARs admit Na^+, elevations of Na^+ might also be involved
291 in cooperative signalling. Also, postsynaptic Na^+ signals could report the activity of the Ca^{2+}-
292 impermeable GC AMPARs and Na_vs in a more direct way than Ca^{2+} signals and thus yield
293 additional information on the state of the locally activated GC spine. We performed two-
294 photon Na^+ imaging using SBFI at a concentration of 1 mM, far below the Na^+ concentration
295 of 15 mM in the internal solution, so the degree of buffering is negligible (Mondragao et al.,
296 2016; settings as in Ona-Jodar et al., 2017; Fig. 5C,D). The ensuing Na^+ signals following
297 TPU of glutamate at individual spine heads with similar parameters as above had a mean
298 amplitude of $-(\Delta F/F)_{TPU}$ = 4.9 ± 1.4 % in the spine head and were localized to the spine head
299 to some extent (signal ratio in adjacent dendrite 0.56 ± 0.38 of spine signal; $P < 0.001$ vs
300 spine signal amplitude; n = 13 spines in 11 GCs). Conversion of the signal amplitude to
301 absolute changes in $[Na^+]_i$ (Rose et al., 1999; Ona-Jodar et al., 2017) yields a mean increase
302 $\Delta[Na^+]_i$ by ~ 10 mM. The average half duration was $\tau_{1/2}$ = 890 ± 770 ms in the spines,
303 including frequently observed plateau phases. Because of the small signal to noise ratio in the
304 individual experiments we also averaged data across all spine/dendrite pairs (Fig. 5C bottom).
305 The averaged spine signal showed an initial plateau phase of 600 ms, and the averaged
306 dendrite signal mirrored the kinetics of the spine signal, which would be expected because of
307 the fast diffusion of Na^+ into the dendrite (Mondragao et al., 2016). The TPU-evoked signals

308 are very slow in view of the fast diffusion of Na^+ and recent data from synaptic signals in
309 hippocampal pyramidal neuron spines (their $\tau_{1/2} \sim 20$ ms; Miyazaki and Ross, 2017).
310 From these experiments we conclude that the time course of the asynchronous component of
311 GABA release triggered by unitary activation matches well with prolonged elevated Na^+ and
312 Ca^{2+} concentrations in the GC spine. Thus late release could result from local processing
313 following unitary inputs to the reciprocal spine (see Discussion).
314

315 ***Discussion***

316 Here we have demonstrated that local uncaging of glutamate onto individual olfactory bulb
317 GC spines can activate the entire microcircuit within the spine, from the local spine spike to
318 the release of GABA onto MC lateral dendrites, which confirms the functionality of the
319 microcircuit as a mini-neuron. As in classical axonal release, Na_v channel and HVACC
320 activation contribute to microcircuit output, which occurs on both fast and slow time scales.
321 The time course of the asynchronous component is matched by postsynaptic Na^+ and Ca^{2+}
322 elevations. Strikingly, however, we observed that NMDA receptors also play a major role in
323 both fast and slow release and that the involved pathway is likely to cooperate with the
324 Na_v/HVACC mediated pathway.

325 *Properties of microcircuit output*

326 For the proximal reciprocal GC inputs investigated here we estimate that under physiological
327 conditions close to the MC resting potential the size of the fast IPSCs is on the order of -5 pA,
328 after corrections for the presence of DNI and the setting of E_{Cl}. Assuming an *in vivo* input
329 resistance of MCs of 100 MΩ (Angelo and Margrie, 2011), a single GC-mediated IPSC will
330 exert a somatic hyperpolarization of at best 0.5 mV. Thus proximal single GC spine inputs are
331 likely to play a rather subtle role in influencing MC firing (Fukunaga et al., 2014; McIntyre
332 and Cleland, 2016), unless there is coordinated activity across GC spines connected to the
333 same MC dendrite, most importantly in the wake of an MC action potential during the
334 recurrent IPSP (see e.g. Fig. 4E), during gamma oscillations (e.g. Kay, 2003; Lagier et al.,
335 2004) or due to 'super-inhibitory connectivity' as predicted by Gilra and Bhalla (2015).

336 A negative correlation between IPSC amplitudes and distance to the soma would be expected
337 because of electrotonic attenuation and from earlier work (Lowe, 2008); our data do not show
338 such an effect, probably due to the close proximity of most stimulation sites to the soma with
339 a mean distance of ~ 20 μm and variability across sizes of individual GABAergic synapses,
340 dendritic input resistance etc.

341 Upon local activation we observed a release probability P_r from the GC spine on the order of
342 0.33. This P_r value might represent an upper limit, because the global reduction of inhibition
343 by DNI might cause homeostatic effects that could also involve an increase in P_r at
344 GABAergic synapses (e.g. Rannals and Kapur, 2011). Moreover there is a general bias for
345 detection of connections with larger P_r due to the high level of spontaneous activity and
346 limited recording time. However, since our experiments were conducted at room temperature,
347 physiological temperatures might counterbalance such effects.
348 Assuming a P_r of 0.3 allows to estimate the efficiency of the entire reciprocal microcircuit
349 based on previous observations of the probability for glutamate release from the MC dendrites
350 on the order of 0.5 – 0.75 (Egger et al., 2005; Pressler and Strowbridge, 2017). Thus the total
351 efficiency of the microcircuit is likely to be on the order of 0.2, possibly informing future
352 network models of bulbar interactions. The rather low P_r for GABA observed here also
353 implies that GC spines might become enabled to release with higher probabilities during a
354 coincidence with global GC signalling (Ca^{2+} spike or global AP), due to increased ΔCa^{2+} in
355 the spine (Egger et al., 2005; Egger, 2008; but see Aghvami et al., manuscript in revision, for
356 sublinear summation effects during perfect coincidence).
357 As to the minimal latency required for release of GABA, the temporal resolution of our
358 experiments is limited by the duration of the uncaging pulse (1 ms) and by not knowing the
359 time course of the membrane potential $V_m(t)$ in the GC spine. Fig. 1E shows that the fastest
360 urIPSCs were detected within 2 ms from TPU onset, implying that there is a fast mechanism
361 coupling Ca^{2+} entry to release as in classical axonal release as suggested previously (Bywalez
362 et al., 2015; Nunes and Kuner, 2018) and also supported by the role of Na_v/HVACC
363 demonstrated here (see below). While ~ 30% of urIPSCs occurred within 10 ms post TPU
364 onset, there was also a substantial fraction with longer latencies in the range of 10 - 30 ms.
365 The fast urIPSCs and possibly also the events with medium latency could still contribute to

366 the aforementionaed gamma oscillations that originate within the MC-GC reciprocal
367 microcircuits.
368 Substantial asynchronous release from the GC spine on yet longer time scales (detected at up
369 to 550 ms post TPU) was frequently observed in our study; while the detailed mechanism for
370 delayed release remains to be elucidated, we found that TPU of glutamate results in elevations
371 of both Ca^{2+} and Na^{+} concentrations within the spine lasting for similar durations (see below).
372 Thus with regard to temporal processing the microcircuit is capable of operating across a wide
373 range of latencies and also of generating combined synchronous and asynchronous output.
374 *Na_v-mediated and NMDAR-mediated contributions to release*
375 How is postsynaptic Ca^{2+} entry coupled to release of GABA within the GC spine? Previously
376 we have shown via occlusion experiments that Ca^{2+} entry via NMDARs occurs independently
377 from Ca^{2+} entry mediated by the Na_v-HVACC pathway, since AMPAR-mediated
378 depolarization on its own is strong enough to lift the Mg^{2+} block, probably due to boosting by
379 the high GC spine neck resistance (Bywalez et al., 2015). Therefore we hypothesized that the
380 Na_v-HVACC pathway would provide the sole trigger for fast release of GABA, as in classical
381 release from axons (see also the recent findings on GC Na_v 1.2 by Nunes and Kuner, 2018),
382 reinforcing the notion of the GC spine as an independent mini-neuron that can generate output
383 without global firing. Indeed, blockade of either Na_v or HVACCs strongly reduced or
384 abolished urIPSCs. However, in subsequent experiments probing NMDAR contribution we
385 observed that urIPSCs became strongly reduced by blockade of NMDARs as well.
386 As a note of caution, activation of single GC spines via TPU might involve spurious
387 activation of extrasynaptic NMDARs since at the large GC spines TPU does not necessarily
388 occur at the precise location of the glutamatergic postsynapse, and we also observed that TPU
389 resulted in a slightly larger NMDA-receptor mediated component of the postsynaptic Ca^{2+}
390 signal than true synaptic activation via glomerular stimulation which was the only significant
391 difference between the two data sets (~ 65 % vs ~ 50%, Bywalez et al., 2015; Egger et al.,

392 2005). Thus at least part of the strong impact of NMDARs observed here might be rooted in
393 such extrasynaptic glutamatergic activation, similar to what is suggested to happen during
394 MC-step on a yet larger scale (see introduction).
395 Therefore we tested for a role of NMDARs in recurrent inhibition elicited by MC APs, and
396 could demonstrate that NMDAR blockade alone (which does not prevent spine spike
397 generation, see Bywalez et al., 2015) also reduces recurrent inhibition. It appears from these
398 experiments that NMDARs are not absolutely necessary for all GABA release events, because
399 recurrent inhibition was not blocked entirely. However, inhibitory feedback from neurons
400 other than GCs could explain part of the APV-resistant component of the rIPSP (see below).
401 In summary, we observe that both Na_vs and NMDARs can contribute to release of GABA in a
402 cooperative manner, the exact mechanism of which remains to be elucidated. Presynaptic
403 actions of NMDARs have been described at other synapses (Bouvier et al., 2015; Dore et al.,
404 2017). If the presumed cooperation was mediated by ΔCa^{2+} itself, this would require a
405 colocalization of NMDARs and HVACCs in the active zone of the GC spine, which remains
406 to be investigated. In addition, because of temporal constraints for the fast release components
407 observed here it is tempting to speculate that NMDAR-mediated Ca^{2+} currents could become
408 activated already before the peak of the spine spike and the ensuing activation of HVACCs,
409 allowing for summation of the respective Ca^{2+} signals.
410 *Further implications of involvement of NMDARs in GABA release*
411 The observation of an apparent cooperation between Na_v/HVACCs and NMDARs relates our
412 study back to the initial studies on dendrodendritic recurrent inhibition, when it was
413 concluded by several groups that NMDARs can contribute directly to release from the
414 reciprocal spine (see Introduction). However, the relative contribution of NMDARs has been
415 under debate. While MC-step, the standard protocol used for evoking dendrodendritic
416 recurrent inhibition of MCs via 20-50 ms long depolarizations, would evoke recurrent
417 inhibition also in the presence of TTX (possibly even enhanced, Halabisky et al., 2000), it

418 was reported by two groups that recurrent inhibition in response to shorter MC-step stimuli (<
419 5 ms) is substantially smaller than for the long MC-step and reduced in TTX (Schoppa et al.,
420 1998; Halabisky et al., 2000). These observations seem to indicate that the standard MC-step
421 protocol recruits NMDAR-dependent pathways for triggering GABA release also via
422 prolonged release of Glu and the subsequent summation of EPSPs in GC spines, whereas
423 short stimulation is more likely to recruit the GC spine spike that we have recently described
424 (Halabisky et al., 2000; Bywalez et al., 2015). Thus a cooperative mechanism could reconcile
425 some of the aforementioned earlier findings. Summation effects could also play a role in
426 physiological signalling, in particular following MC theta bursts as observed during odor
427 sampling *in vivo*.
428 Finally, another interesting aspect of the strong influence of NMDARs is that this property is
429 likely to differentiate the MC-GC microcircuit from the MC-parvalbumin cell microcircuit.
430 Since PV+ cells feature Ca^{2+}-permeable AMPARs and show a rather small NMDAR
431 component in response to MTC input (Kato et al., 2013), the strong effect of APV on urIPSCs
432 here argues in favor of a preferential activation of the MC-GC circuit by our experimental
433 method, along with the proximal stimulation and the use of VGAT-Venus rats. Conversely,
434 inhibitory feedback from neurons other than GCs could also explain part of the APV-resistant
435 component of the rIPSP (Fig. 4E).
436 *Asynchronous release and postsynaptically elevated Ca^{2+} and Na^{+} in the spine head*
437 Asynchronous release – i.e. release that happens later than the fast coupling of HVA
438 presynaptic Ca^{2+} currents to the release machinery (e.g. Kaeser and Regehr, 2013) - is a
439 phenomenon known from from many central synapses. It is often observed at repetitively
440 stimulated synapses (Wen et al., 2013), which would also hold for the MC-step protocol,
441 where ongoing release of glutamate from MCs is likely to happen over dozens of ms and
442 subsequent asynchronous release of GABA has been documented by many groups (see
443 Introduction). Thus it was at first surprising that local stimulation would suffice to elicit

444 asynchronous release. However, the temporal extent of asynchronous release observed here
445 was shorter than in the classical MC-step experiments (> 1 s vs a maximal extent of ~ 500 ms
446 here) and therefore there might be additional mechanisms involved whenever GCs are
447 activated more strongly.
448 NMDAR-mediated Ca^{2+} entry in itself is expected to recede on the order of 100 ms and thus
449 on its own is unlikely to mediate asynchronous release far beyond the first 100 ms; Na_v-
450 mediated Ca^{2+} entry via HVACCs should decline even faster. To further unravel signalling
451 downstream of the NMDAR and Na_v and thus move towards unravelling both the
452 mechanisms of cooperativity and asynchronous release we investigated the time course of
453 postsynaptic Na^+ and Ca^{2+} elevations with minimal exogenous buffering. Both ion species
454 showed elevated levels for durations well compatible with asynchronous output. In particular,
455 there was a substantial and long-lasting postsynaptic elevation of Na^+. This detected $\Delta[Na^+]_i$ is
456 much higher than what could be extrapolated for a single backpropagating GC AP (~ 1 mM,
457 Ona-Jodar et al., 2017). Thus there must be substantial Na^+ entry via AMPARs and NMDARs
458 and possibly other postsynaptic sources. The elevation of $[Na^+]_i$ persisted during a plateau-
459 like phase, very much unlike recent observations of synaptic Na^+ transients in spines of
460 hippocampal pyramidal neurons which decayed within 20 ms (Miyazaki and Ross, 2017). The
461 slow decay of the GC spine $\Delta[Na^+]_i$ might be explained by the diffusive barrier provided by
462 the high neck resistance (predicted as ≥ 1GΩ, Bywalez et al., 2015). At this point we can only
463 speculate about the origin of the plateau. It might correspond to a local UP state in the GC
464 spine which causes a reversal of the pumping activity of the Na^+/Ca^{2+}-exchanger, similar to a
465 model recently proposed for apical dendritic tufts of MCs of the accessory olfactory bulb
466 (Zylbertal et al., 2015). Such a reverse action might then provide ongoing local influx of Ca^{2+}
467 sufficient to trigger release. This influx should also happen close to the release machinery,
468 since buffering of GC Ca^{2+} by EGTA had no effect on asynchronous release (Isaacson, 2001).
469 The UP state might not be evident in GC somatic membrane potential recordings due to

470 filtering by the spine neck resistance. Increased $[Na^+]_i$ within the observed regime might also
471 provide positive feedback to NMDARs via an upregulation of NMDAR Ca^{2+} currents by the
472 Src kinase (Yu and Salter, 1997, 1998). Further experiments are required to unravel such
473 interactions.

474 *Sources of spontaneous inhibitory activity in mitral cells*

475 The MC apical tuft is thought to contribute to the high level of spontaneous activity mostly
476 via excitatory inputs that also can provide lateral excitation between the tufts of sister mitral
477 MCs within the same glomerulus (Schoppa et al., 2001; Christie and Westbrook, 2006;
478 Pimentel and Margrie, 2008). MCs with truncated tufts do not show a reduced sIPSC
479 frequency (Arnson and Strowbridge, 2017) but are less prone to exhibit long-lasting
480 depolarizations (LLDs) and excitation via metabotropic GluRs (Carlson et al., 2000; Dong et
481 al., 2008). We observed that all three antagonists of urIPSC generation (TTX, CTX, APV)
482 also substantially reduced spontaneous IPSC frequency (to 15%, 50% and 35% of control,
483 respectively. In the case of Na_v blockade, strong effects are to be expected because of the
484 blockade of spontaneous firing and thus a decrease in the excitation levels also of inhibitory
485 neurons (GCs and other lateral inputs alike). Moreover, as we have shown above,
486 spontaneous release of glutamate from MC lateral dendrites onto GC spines is far less likely
487 to trigger recurrent release in the presence of TTX because of blockade of the spine spike.
488 Other groups have observed similarly strong effects of TTX on sIPSC frequency (e.g.
489 Halabisky et al., 2000; Arnson and Strowbridge, 2017). The effect of HVACC blockade alone
490 was less pronounced than for TTX, because it will neither prevent spontaneous spikes nor
491 spontaneous release of vesicles and thus have less of an effect on global network activity.

492 The substantial effect of NMDAR blockade on spontaneous IPSCs was also observed in other
493 olfactory bulb studies (Wellis and Kauer, 1993; Schmidt and Strowbridge, 2014). Part of the
494 strong contribution of NMDARs to bulbar network activity may be related to the LLDs
495 observed in MCs. While these LLDs do not require NMDARs to become triggered, they are

496 enhanced in amplitude and duration via NMDARs (Carlson and Keller, 2000) and in our
497 hands often increased their frequency in the presence of DNI-caged glutamate. In addition,
498 MC NMDA autoreceptors will also contribute (see Introduction). Finally, the contribution of
499 NMDARs to release from the GC spine observed here also implies that in the presence of
500 APV spontaneous release of glutamate from MCs is less likely to trigger MC-GC rIPSCs.

501 *Functional role of local reciprocal processing*

502 While there is first evidence for substantial dendritic Ca^{2+} signals and local GC spine signals
503 *in vivo* (Wienisch et al., 2016; Wallace et al., 2017; Zhang et al., 2016), the extent to which
504 specifically local GABA release from GC spines contributes to odor processing in the
505 olfactory bulb is difficult to estimate at this point. Athough it is very likely that global GC
506 spiking is not required for the generation of gamma oscillations (Lagier et al., 2004), the
507 precise role of gamma in odor processing is not yet clear. Further advances in high resolution
508 functional imaging including further development of voltage-sensitive dyes might be required
509 to tackle these questions. Genetic loss-of-function approaches would need to either
510 exclusively prevent global signals in GCs (but not the spine spike) or to come up with
511 methods to inactivate GABA release from all the GC spines associated with one particular
512 glomerular set of MCs but not from the other spines, such that the impact of recurrent
513 inhibition could be separated from the lateral inhibition which requires global GC activity.

514 In any case, there is convincing evidence for a role of both NMDARs and Na_vs specifically in
515 difficult odor discriminations, since in the same behavioral paradigm GC-specific knock-
516 down (in about ~50% of GCs) of GluN1 resulted in an increase in discrimination time of on
517 average ~ 60ms, and of Na_vs of ~ 85 ms versus control, while simple discriminations were not
518 affected (Abraham et al., 2010; Nunes and Kuner, 2018).

519 **Experimental procedures**

520 *Animal handling, slice preparation and electrophysiology*

521 Animals used in our experiments were juvenile Wistar or VGAT-Venus transgenic rats
522 (VGAT-Venus /w-Tg(SLc32a1-YFP*)1Yyan) of either sex (P11 – P19). VGAT-Venus
523 transgenic rats are based on mouse BAC transgenic lines. They were generated by Drs. Y.
524 Yanagawa, M. Hirabayashi and Y. Kawaguchi at the National Institute for Physiological
525 Sciences, Okazaki, Japan, using pCS2-Venus provided by Dr. A. Miyawaki (Uematsu et al.,
526 2008), RRID: RGD_2314361. In this rat line, fluorescent Venus protein is preferentially
527 expressed in cells carrying the vesicular GABA transporter (VGAT), i.e. GABAergic
528 neurons: the localization of Venus-labeled cells across OB layers was found to be similar to
529 that of GABA-positive cells; direct colocalization in the cortex yielded an overlap of 97%
530 (Uematsu et al., 2008).

531 Sagittal olfactory bulb brain slices (thickness 300 µm) were prepared in ACSF (composition
532 see below) following procedures in accordance with the rules laid down by the EC Council
533 Directive (86/89/ECC) and German animal welfare legislation. Slices were incubated a water
534 bath at 33°C for 30 min and then kept at room temperature (22°C) until recordings were
535 performed.

536 <u>Mitral cell experiments</u>

537 Olfactory bulb mitral cells were visualized by gradient contrast and recorded from in whole
538 cell voltage clamp mode (at -70 mV or +10 mV) or current clamp mode. Recordings were
539 made with an EPC-10 amplifier and Patchmaster v2.60 software (both HEKA Elektronik,
540 Lambrecht/Pfalz, Germany). Experiments were performed at room temperature (22°C). Patch
541 pipette resistance ranged from 5-6-MΩ. Mitral cells clamped at -70 mV were filled with
542 intracellular solution containing the following substances (in mM): (1) tip solution: 130 K-
543 Methylsulfate, 10 HEPES, 4 MgCl2, 2 Ascorbic acid, 10 Phosphocreatine-di-tris-salt, 2.5
544 Na2ATP, 0.4 NaGTP (2) backfilling solution: 110 Cs-Chloride, 10 HEPES, 10 TEA,

545 4MgCl2, 2 Ascorbic acid, 10 5-N-(2,6-dimethylphenylcarbamoylmethyl) triethylammonium
546 bromide (QX-314, Sigma), 0.2 EGTA, 10 Phosphocreatine, 2.5 Na2ATP, 0.4 NaGTP. Mitral
547 cells clamped at + 10mV contained internal solution composed of: 125 Cs-methanesulfonate
548 1 NaCl, 0.5 EGTA, 10 HEPES, 3 MgATP, 0.3 NaGTP, 10 Phosphocreatine-di-Tris-salt,
549 10QX-314, 0.05 Alexa 594 (Ca^{2+} indicator, Thermofisher Scientific, Waltham.
550 Massachusetts, US), at pH 7.3. For mitral cell current clamp experiments the same internal
551 solution as for granule cell current clamp experiments was used, but without fluorescent dye
552 (see below). APs were evoked by somatic current injection (3 ms, 1 nA) and 5 APs were
553 elicited for every recording condition.
554 The extracellular ACSF was bubbled with carbogen and contained (in mM): 125 NaCl, 26
555 $NaHCO_3$, 1.25 NaH_2PO_4, 20 glucose, 2.5 KCl, 1 $MgCl_2$, and 2 $CaCl_2$. The following
556 pharmacological agents were bath-applied in some experiments: bicucculline (BCC, 50 µM,
557 Sigma-Aldrich), ω-conotoxin MVIIC (CTX, 1 µM, Alomone, Jerusalem, Israel), TTX (500
558 nM, Alomone), D-APV (25 µM, Tocris). In pharmacological experiments we waited for 10
559 minutes after wash-in of the drugs TTX, APV resp. CTX. In CTX experiments 1mg/ml
560 cyctochrome C was added to the ACSF. TTX voltage clamp experiments were conducted at
561 clamping potentials of -70 mV (n = 5) or + 10 mV (n = 7), whereas all APV and CTX voltage
562 clamp experiments were conducted at + 10 mV.
563 Granule cell experiments (Na^+ and Ca^{2+} imaging)
564 Whole cell current clamp recordings were performed at room temperature (22°C) and granule
565 cells were held near their resting potential of below -70 mV. Granule cells were filled with an
566 internal solution containing the following substances (in mM): 130 K-Methylsulfate, 10
567 HEPES, 4 MgCl2, 2 Ascorbic acid, 10 Phosphocreatine-di-tris-salt, 2.5 Na2ATP, 0.4 NaGTP,
568 and 1 mM SBFI (sodium-binding benzofuran isophthalate, Teflabs, Austin, TX and
569 Molecular Probes, Eugene, OR, USA) or 0.1 OGB-6F (Ca^{2+} indicator, Thermofisher
570 Scientific, Waltham. Massachusetts, USA). The patch pipette resistance varied between 6 and

571 7 MΩ. The ACSF was the same as for mitral cell experiments.

572 *Combined two-photon imaging and uncaging*

573 Imaging and uncaging were performed on a Femto-2D-uncage microscope (Femtonics,
574 Budapest, Hungary). Two tunable, Verdi-pumped Ti:Sa lasers (Chameleon Ultra I and II
575 respectively, Coherent, Santa Clara, CA, USA) were used in parallel. The first laser was set
576 either to 900 nm for simultaneous excitation of YFP and Alexa 594 in one channel for
577 visualization of spines and the mitral cell for urIPSC recordings, to 840 nm for excitation of
578 OGB-6F or to 800 nm for excitation of SBFI in GC spines and dendrites, and the second laser
579 was set to 750 nm for uncaging of caged glutamate. The two laser lines were directly coupled
580 into the pathway of the microscope with a polarization cube (PBS102, Thorlabs Inc, Newton,
581 NJ, USA) and two motorized mirrors. As caged compound we used DNI-caged glutamate
582 (DNI; Femtonics). DNI was used in 1 mM concentration in a closed perfusion circuit with a
583 total volume of 12 ml. Caged compounds were washed in for at least 10 minutes before
584 starting measurements. The uncaging laser was switched using an electro-optical modulator
585 (Pockels cell model 350-80, Conoptics, Danbury, CT, USA). The emitted fluorescence was
586 split into a red and a green channel with a dichroic mirror.

587 Triggering of mitral cell reciprocal IPSCs

588 The region of interest on a proximal lateral mitral cell dendrite was moved to the center of the
589 scanning field. Four uncaging spots were placed in close apposition along the lateral mitral
590 cell dendrite in case of 'blind' uncaging or one spot was positioned near the region of interest
591 when YFP fluorescence of GABAergic cells in VGAT-Venus rats was used as an optical help
592 to identify potential synaptic contacts between mitral cell lateral dendrites and granule cell
593 spines.

594 The uncaging power was adjusted to the depth of the measured region of interest,
595 corresponding to a laser power of approximately 15 mW at the uncaging site (Sobczyk et al.,
596 2005). The uncaging beam was positioned at ~ 0.2 - 0.5 µm distance from the mitral cell

597 dendrite/ potential site of synaptic MC – GC contact. The uncaging pulse duration was 1 ms.
598 The scanning position was readjusted if necessary before each measurement to account for
599 drift. The microscope was equipped with a 60x Nikon Fluor water immersion objective (NA
600 1.0; Nikon Instruments, Tokyo, Japan). The microscope was controlled by MES v.5.3190
601 software (Femtonics).

602 *Uncaging stability*

603 To test for the stability of uncaging evoked recurrent IPSCs in mitral cells, uncaging at a
604 dendritic region of interest was performed. If uncaging led to the repetitive occurrence of an
605 urIPSC in the same time window, the stability measurement was continued by either uncaging
606 30 times in total with a frequency of 0.033 Hz or 5 times in a row with 0.033 Hz followed by
607 a 10 min break (to mimic the time for wash-in of pharmacological compounds) and another
608 round of uncaging (5x, 0.033Hz). urIPSC amplitudes were taken from averages of the first 5 –
609 10 and the last 5 – 10 uncaging sweeps and statistically compared with each other.

610 *Na^+ or Ca^{2+} imaging of granule cell spines and simultaneous glutamate uncaging*

611 For Na^+ imaging experiments, electrophysiology and imaging were performed as in (Ona-
612 Jodar et al., 2017), and for Ca^{2+} imaging experiments as in (Bywalez et al., 2015). Two-
613 photon uncaging of glutamate was performed as described above and in (Bywalez et al.,
614 2015). Na^+ and Ca^{2+} signals were imaged in line scanning mode with a temporal resolution of
615 ~ 1 ms. The scan position was checked and readjusted if necessary before each measurement
616 to account for drift.

617 *Data analysis and statistics*

618 Electrophysiological and imaging data were analysed with custom written macros in Igor pro
619 (Wavemetrics, Lake Oswego, OR, USA). Additional sIPSC and urIPSC analysis was
620 performed using the Mini Analysis program (Synaptosoft, Decature, GA, USA) and Origin
621 (Northampton, MA, USA).

622 Detection of urISPCs Due to the high spontaneous activity, in order to test for the presence of
623 a signal we performed first an area and event analysis of IPSC traces (see below and Fig. 1D;
624 if a signal was detected based on these analyses we went on to search for individual triggered
625 urIPSCs by visual inspection of an overlay of the recorded traces. Individual IPSCs were
626 considered as uncaging-evoked when they repetitively occurred within the same time window
627 (3 ± 2 ms, n = 31) after uncaging and had similar kinetics (indicating a similar location of the
628 respective input on the dendrite). Signal types ranged from single urIPSC events to barrages
629 of urIPSCs lasting tens to hundreds of ms. The time span of signals was measured in averaged
630 responses as the duration from the onset until the return to the baseline (Fig. S1D2).
631 The release probability was estimated based on 5 – 30 TPU samplings with a mean of 7.5
632 ±1.7 stimulations (n = 31).
633 Area analysis The area was measured as the integrated activity above baseline for a 500 ms
634 pre-uncaging baseline window and for a post-uncaging window in individual traces to screen
635 for the presence of a signal (Fig. 1D). The 500 ms extent of the time windows was validated
636 by our measurements of averaged barrage duration (see Fig. S1D2).
637 Delta (Δ) area values were calculated by subtracting the area of a 500 ms pre-uncaging
638 baseline window ('pre') from a 500 ms post-uncaging window ('post'), to isolate the amount
639 of uncaging-evoked inhibitory activity from spontaneous activity. If this procedure was
640 applied to averaged traces and the result was negative, the Δ area value was set to zero (i.e. no
641 uncaging-evoked activity). While this procedure might still generate false positives due to
642 spontaneous bursts of activity in the post-uncaging window, it also prevents a spurious
643 cancelling of activity during averaging across experiments. Δ area values for pharmacological
644 conditions were normalized to control Δ area in order to assess the net effect of drugs on
645 uncaging-evoked inhibitory activity (Fig. 2D, 3D, 4D).
646 Event analysis Within the individual recorded traces, the peak time points of individual IPSCs
647 were analysed. Peak search parameters in MiniAnalysis were adjusted in order to detect

648 potentially all IPSCs within a trace. For detailed spontaneous IPSC amplitude analysis, IPSCs
649 were sorted manually after the automated peak search and discarded if the amplitude
650 exceeded less than 5 pA and/or the amplitude onset was not detected properly. Event counts
651 were averaged for the 500 ms pre-uncaging and the 500 ms post-uncaging windows,
652 respectively.

653 Evaluation of effects of pharmacological agents For determining drug effects, the averaged
654 urIPSC amplitudes were scaled by the ratio of number of responses to total number of trials,
655 both in control and drug condition, in order to account also for changes in release probability.
656 If no single responses/urIPSCs could be detected anymore in the presence of TTX, CTX or
657 APV according to the criteria described above, we measured the mean amplitude of V_m above
658 baseline in the averaged response at the time point of the maximal response amplitude in
659 control condition. If this value was below 0, the response size was set to 0 pA. If the value
660 was larger than 0, we interpreted it as average drug response amplitude including failures and
661 thus did not scale it. This conservative method prevents false negatives due to lacking
662 sensitivity in individual trials in the presence of the drug.

663 Detection of spontaneous activity Spontaneous IPSCs were recorded prior to wash-in of DNI,
664 in the presence of DNI and in the presence of each pharmacological compound. For each
665 condition, data were analysed for a total duration of 20 s of recordings.

666 Analysis of recurrent IPSPs For each recording, the amplitude was measured as the maximal
667 negative deflection of the membrane potential from baseline, the half duration of decay $\tau_{1/2}$ as
668 the time between the time point of the maximal amplitude and its decay to half the maximal
669 value and the total duration as the time span between the onset of the hyperpolarization below
670 baseline and return to baseline. Values for all 5 recordings in one condition were averaged.

671 Statistical tests Data were analysed with non-parametric paired (*Wilcoxon matched* pairs) or
672 unpaired (*Mann-Whitney-U*) tests and expressed as mean ± SD.

673

674 ***Author contributions***

675 VR performed all experiments, except for granule cell Na^+ imaging by TOJ, mitral cell curent
676 clamp experiments by GY and initial test experiments by VE. VR, TOJ, GY and VE analyzed
677 data. VE and VR designed research and wrote the manuscript. BR provided DNI-caged
678 glutamate, and all co-authors except for GY contributed to editing the manuscript.

679 ***Acknowledgments***

680 We thank Anne Pietryga-Krieger for expert technical assistance, Christine R. Rose and Niklas
681 Gerkau for the introduction to Na^+ imaging, Marius Stephan and Philipp Seidel for assistance
682 with IPSC analysis, Imre Vida for facilitating access to VGAT-Venus rats and Christine R.
683 Rose for comments on the manuscript. This work was funded mainly by the German Federal
684 Ministry for Education and Research (BMBF, 01GQ1104/01GQ1502, V.E.), with additional
685 equipment funding by LMU-GSN and DFG-SFB 870.

686 ***Competing interests***

687 There are competing financial interests since B.R. is a founder of Femtonics Kft and a
688 member of its scientific advisory board. No other competing interests exist.

689

690 ***References***

691 Abraham, N. M., Egger, V., Shimshek, D. R., Renden, R., Fukunaga, I., Sprengel, R., Seeburg, P. H.,
692 Klugmann, M., Margrie, T. W., Schaefer, A. T., & Kuner, T. (2010). Synaptic inhibition in
693 the olfactory bulb accelerates odor discrimination in mice. *Neuron, 65*(3), 399-411.
694
695 Angelo, K., & Margrie, T. W. (2011). Population diversity and function of hyperpolarization-
696 activated current in olfactory bulb mitral cells. *Sci Rep, 1*, 50. doi:10.1038/srep00050
697
698 Arnson, H. A., & Strowbridge, B. (2017). Spatial Structure Of Synchronized Inhibition In The
699 Olfactory Bulb. *J Neurosci,* 37(43):10468 –10480. doi:10.1523/JNEUROSCI.1004-17.2017
700
701 Aroniadou-Anderjaska, V., Ennis, M., & Shipley, M. T. (1999). Dendrodendritic recurrent excitation
702 in mitral cells of the rat olfactory bulb. *J Neurophysiol, 82*(1), 489-494.
703 doi:10.1152/jn.1999.82.1.489
704
705 Bartel, D. L., Rela, L., Hsieh, L., & Greer, C. A. (2015). Dendrodendritic synapses in the mouse
706 olfactory bulb external plexiform layer. *J Comp Neurol, 523*(8), 1145-1161.
707 doi:10.1002/cne.23714
708
709 Bloodgood, B. L., & Sabatini, B. L. (2007). Ca(2+) signaling in dendritic spines. *Curr Opin*
710 *Neurobiol, 17*(3), 345-351. doi:10.1016/j.conb.2007.04.003
711
712 Bouvier, G., Bidoret, C., Casado, M., & Paoletti, P. (2015). Presynaptic NMDA receptors: Roles and
713 rules. *Neuroscience, 311*, 322-340. doi:10.1016/j.neuroscience.2015.10.033
714
715 Bywalez, W. G., Patirniche, D., Rupprecht, V., Stemmler, M., Herz, A. V. M., Pálfi, D., Rozsa, B., &
716 Egger, V. (2015). Local Postsynaptic Voltage-Gated Sodium Channel Activation in Dendritic
717 Spines of Olfactory Bulb Granule Cells. *Neuron, 85*(3), 590-601.
718 doi:10.1016/j.neuron.2014.12.051
719
720 Carlson, G. C., Shipley, M. T., & Keller, A. (2000). Long-lasting depolarizations in mitral cells of the
721 rat olfactory bulb. *J Neurosci, 20*(5), 2011-2021.
722
723 Chen, W. R., Xiong, W., & Shepherd, G. M. (2000). Analysis of relations between NMDA receptors
724 and GABA release at olfactory bulb reciprocal synapses. *Neuron, 25*(3), 625-633.
725
726 Chiovini, B., Turi, G. F., Katona, G., Kaszas, A., Palfi, D., Maak, P., Szalay, G., Szabo, M. F., Szabo,
727 G., Szadai, Z., Kali, S., & Rozsa, B. (2014). Dendritic spikes induce ripples in parvalbumin
728 interneurons during hippocampal sharp waves. *Neuron, 82*(4), 908-924.
729 doi:10.1016/j.neuron.2014.04.004
730
731 Christie, J. M., & Westbrook, G. L. (2006). Lateral excitation within the olfactory bulb. *J Neurosci,*
732 *26*(8), 2269-2277.
733
734 Didier, A., Carleton, A., Bjaalie, J. G., Vincent, J. D., Ottersen, O. P., Storm-Mathisen, J., & Lledo, P.
735 M. (2001). A dendrodendritic reciprocal synapse provides a recurrent excitatory connection in
736 the olfactory bulb. *Proc Natl Acad Sci U S A, 98*(11), 6441-6446.
737
738 Dong, H. W., Hayar, A., & Ennis, M. (2007). Activation of group I metabotropic glutamate receptors
739 on main olfactory bulb granule cells and periglomerular cells enhances synaptic inhibition of

mitral cells. *J Neurosci, 27*(21), 5654-5663.

Egger, V. (2008). Synaptic sodium spikes trigger long-lasting depolarizations and slow calcium entry in rat olfactory bulb granule cells. *Eur J Neurosci, 27*(8), 2066-2075.

Egger, V., Nevian, T., & Bruno, R. M. (2007). Subcolumnar Dendritic and Axonal Organization of Spiny Stellate and Star Pyramid Neurons within a Barrel in Rat Somatosensory Cortex. *Cereb Cortex*.

Egger, V., & Stroh, O. (2009). Calcium buffering in rodent olfactory bulb granule cells and mitral cells. *J Physiol, 587*(Pt 18), 4467-4479.

Egger, V., Svoboda, K., & Mainen, Z. F. (2005). Dendrodendritic synaptic signals in olfactory bulb granule cells: Local spine boost and global low-threshold spike. *J Neurosci, 25*, 3521-3530.

Egger, V., & Urban, N. N. (2006). Dynamic connectivity in the mitral cell-granule cell microcircuit. *Semin Cell Dev Biol, 17*(4), 424-432.

Fino, E., Araya, R., Peterka, D. S., Salierno, M., Etchenique, R., & Yuste, R. (2009). RuBi-Glutamate: Two-Photon and Visible-Light Photoactivation of Neurons and Dendritic spines. *Front Neural Circuits, 3*, 2. doi:10.3389/neuro.04.002.2009

Friedman, D., & Strowbridge, B. W. (2000). Functional role of NMDA autoreceptors in olfactory mitral cells. *J Neurophysiol, 84*(1), 39-50. doi:10.1152/jn.2000.84.1.39

Fukunaga, I., Herb, J. T., Kollo, M., Boyden, E. S., & Schaefer, A. T. (2014). Independent control of gamma and theta activity by distinct interneuron networks in the olfactory bulb. *Nat Neurosci, 17*(9), 1208-1216. doi:10.1038/nn.3760

Gilra, A., & Bhalla, U. S. (2015). Bulbar Microcircuit Model Predicts Connectivity and Roles of Interneurons in Odor Coding. *PLoS ONE, 10*(5), e0098045. doi:10.1371/journal.pone.0098045

Halabisky, B., Friedman, D., Radojicic, M., & Strowbridge, B. W. (2000). Calcium influx through NMDA receptors directly evokes GABA release in olfactory bulb granule cells. *J Neurosci, 20*(13), 5124-5134.

Huang, L., Garcia, I., Jen, H.-I., & Arenkiel, B. R. (2013). Reciprocal connectivity between mitral cells and external plexiform layer interneurons in the mouse olfactory bulb. *Frontiers in Neural Circuits, 7*. doi:10.3389/fncir.2013.00032

Isaacson, J. S. (1999). Glutamate spillover mediates excitatory transmission in the rat olfactory bulb. *Neuron, 23*(2), 377-384.

Isaacson, J. S. (2001). Mechanisms governing dendritic gamma-aminobutyric acid (GABA) release in the rat olfactory bulb. *Proc Natl Acad Sci U S A, 98*(1), 337-342.

Isaacson, J. S., & Strowbridge, B. W. (1998). Olfactory reciprocal synapses: dendritic signaling in the CNS. *Neuron, 20*(4), 749-761.

Kaeser, P. S., & Regehr, W. G. (2014). Molecular mechanisms for synchronous, asynchronous, and

spontaneous neurotransmitter release. *Annu Rev Physiol, 76*, 333-363. doi:10.1146/annurev-physiol-021113-170338

Kapoor, V., & Urban, N. N. (2006). Glomerulus-specific, long-latency activity in the olfactory bulb granule cell network. *J Neurosci, 26*, 11706-11719.

Kato, H. K., Gillet, S. N., Peters, A. J., Isaacson, J. S., & Komiyama, T. (2013). Parvalbumin-expressing interneurons linearly control olfactory bulb output. *Neuron, 80*(5), 10.1016/j.neuron.2013.1008.1036. doi:10.1016/j.neuron.2013.08.036

Kay, L. M. (2003). Two species of gamma oscillations in the olfactory bulb: dependence on behavioral state and synaptic interactions. *J Integr Neurosci, 2*(1), 31-44.

Lepousez, G., Csaba, Z., Bernard, V., Loudes, C., Videau, C., Lacombe, J., Epelbaum, J., & Viollet, C. (2010). Somatostatin interneurons delineate the inner part of the external plexiform layer in the mouse main olfactory bulb. *J Comp Neurol, 518*(11), 1976-1994. doi:10.1002/cne.22317

Lowe, G. (2002). Inhibition of backpropagating action potentials in mitral cell secondary dendrites. *J Neurophysiol, 88*(1), 64-85.

McIntyre, A. B. R., & Cleland, T. A. (2016). Biophysical constraints on lateral inhibition in the olfactory bulb. *Journal of Neurophysiology, 115*(6), 2937-2949. doi:10.1152/jn.00671.2015

Miller, J. P., Rall, W., & Rinzel, J. (1985). Synaptic amplification by active membrane in dendritic spines. *Brain Res, 325*(1-2), 325-330.

Miyamichi, K., Shlomai-Fuchs, Y., Shu, M., Weissbourd, B. C., Luo, L., & Mizrahi, A. (2013). Dissecting Local Circuits: Parvalbumin Interneurons Underlie Broad Feedback Control of Olfactory Bulb Output. *Neuron, 80*(5), 1232-1245. doi:10.1016/j.neuron.2013.08.027

Miyazaki, K., & Ross, W. N. (2017). Sodium Dynamics in Pyramidal Neuron Dendritic Spines: Synaptically Evoked Entry Predominantly through AMPA Receptors and Removal by Diffusion. *The Journal of Neuroscience, 37*(41), 9964-9976. doi:10.1523/JNEUROSCI.1758-17.2017

Mondragao, M. A., Schmidt, H., Kleinhans, C., Langer, J., Kafitz, K. W., & Rose, C. R. (2016). Extrusion versus diffusion: mechanisms for recovery from sodium loads in mouse CA1 pyramidal neurons. *J Physiol, 594*(19), 5507-5527. doi:10.1113/JP272431

Nunes, D., & Kuner, T. (2018). Axonal sodium channel NaV1.2 drives granule cell dendritic GABA release and rapid odor discrimination. *PLoS Biol, 16*(8), e2003816. doi:10.1371/journal.pbio.2003816

Ona-Jodar, T., Gerkau, N. J., Sara Aghvami, S., Rose, C. R., & Egger, V. (2017). Two-Photon Na(+) Imaging Reports Somatically Evoked Action Potentials in Rat Olfactory Bulb Mitral and Granule Cell Neurites. *Frontiers in Cellular Neuroscience, 11*, 50. doi:10.3389/fncel.2017.00050

Pimentel, D. O., & Margrie, T. W. (2008). Glutamatergic transmission and plasticity between olfactory bulb mitral cells. *J Physiol, 586*(8), 2107-2119.

Pressler, R. T., & Strowbridge, B. W. (2017). Direct Recording of Dendrodendritic Excitation in the Olfactory Bulb: Divergent Properties of Local and External Glutamatergic Inputs Govern Synaptic Integration in Granule Cells. *J Neurosci, 37*(49), 11774-11788. doi:10.1523/JNEUROSCI.2033-17.2017

Rannals, M. D., & Kapur, J. (2011). Homeostatic strengthening of inhibitory synapses is mediated by the accumulation of GABA(A) receptors. *J Neurosci, 31*(48), 17701-17712. doi:10.1523/JNEUROSCI.4476-11.2011

Rose, C. R., Kovalchuk, Y., Eilers, J., & Konnerth, A. (1999). Two-photon Na+ imaging in spines and fine dendrites of central neurons. *Pflugers Arch, 439*(1-2), 201-207.

Sailor, Kurt A., Valley, Matthew T., Wiechert, Martin T., Riecke, H., Sun, Gerald J., Adams, W., . . . Lledo, P.-M. (2016). Persistent Structural Plasticity Optimizes Sensory Information Processing in the Olfactory Bulb. *Neuron, 91*(2), 384-396. doi:http://dx.doi.org/10.1016/j.neuron.2016.06.004

Salin, P. A., Lledo, P. M., Vincent, J. D., & Charpak, S. (2001). Dendritic glutamate autoreceptors modulate signal processing in rat mitral cells. *J Neurophysiol, 85*(3), 1275-1282.

Sassoe-Pognetto, M., Utvik, J. K., Camoletto, P., Watanabe, M., Stephenson, F. A., Bredt, D. S., & Ottersen, O. P. (2003). Organization of postsynaptic density proteins and glutamate receptors in axodendritic and dendrodendritic synapses of the rat olfactory bulb. *J Comp Neurol, 463*(3), 237-248.

Schmidt, L. J., & Strowbridge, B. W. (2014). Modulation of olfactory bulb network activity by serotonin: synchronous inhibition of mitral cells mediated by spatially localized GABAergic microcircuits. *Learn Mem, 21*(8), 406-416. doi:10.1101/lm.035659.114

Schoppa, N. E., Kinzie, J. M., Sahara, Y., Segerson, T. P., & Westbrook, G. L. (1998). Dendrodendritic inhibition in the olfactory bulb is driven by NMDA receptors. *J Neurosci, 18*(17), 6790-6802.

Schoppa, N. E., & Westbrook, G. L. (1999). Regulation of synaptic timing in the olfactory bulb by an A-type potassium current. *Nat Neurosci, 2*(12), 1106-1113.

Schoppa, N. E., & Westbrook, G. L. (2001). Glomerulus-specific synchronization of mitral cells in the olfactory bulb. *Neuron, 31*(4), 639-651.

Shepherd, G. M., & Greer, C. A. (2004). Olfactory bulb. In G. M. Shepherd (Ed.), *The Synaptic Organization of the Brain* (3rd ed., pp. 133-169). New York: Oxford University Press.

Sobczyk, A., Scheuss, V., & Svoboda, K. (2005). NMDA receptor subunit-dependent [Ca2+] signaling in individual hippocampal dendritic spines. *J Neurosci, 25*(26), 6037-6046. doi:10.1523/JNEUROSCI.1221-05.2005

Spruston, N. (2008). Pyramidal neurons: dendritic structure and synaptic integration. *Nat Rev Neurosci, 9*(3), 206-221. doi:10.1038/nrn2286

Stroh, O., Freichel, M., Kretz, O., Birnbaumer, L., Hartmann, J., & Egger, V. (2012). NMDA-receptor dependent synaptic activation of TRPC channels in olfactory bulb granule cells. *The*

Journal of Neuroscience, 32(17), 5737-5746. doi:10.1523/JNEUROSCI.3753-11.2012

Toida, K., Kosaka, K., Heizmann, C. W., & Kosaka, T. (1994). Synaptic contacts between mitral/tufted cells and GABAergic neurons containing calcium-binding protein parvalbumin in the rat olfactory bulb, with special reference to reciprocal synapses between them. *Brain Res, 650*(2), 347-352.

Uematsu, M., Hirai, Y., Karube, F., Ebihara, S., Kato, M., Abe, K., . . . Kawaguchi, Y. (2008). Quantitative Chemical Composition of Cortical GABAergic Neurons Revealed in Transgenic Venus-Expressing Rats. *Cerebral Cortex, 18*(2), 315-330. doi:10.1093/cercor/bhm056

Wallace, J. L., Wienisch, M., & Murthy, V. N. (2017). Development and Refinement of Functional Properties of Adult-Born Neurons. *Neuron, 96*(4), 883-896.e887. doi:10.1016/j.neuron.2017.09.039

Wellis, D. P., & Kauer, J. S. (1993). GABAA and glutamate receptor involvement in dendrodendritic synaptic interactions from salamander olfactory bulb. *J Physiol, 469*, 315-339.

Wen, H., Hubbard, J. M., Rakela, B., Linhoff, M. W., Mandel, G., & Brehm, P. (2013). Synchronous and asynchronous modes of synaptic transmission utilize different calcium sources. *Elife, 2*, e01206. doi:10.7554/eLife.01206

Wienisch, M., & Murthy, V. N. (2016). Population imaging at subcellular resolution supports specific and local inhibition by granule cells in the olfactory bulb. *Scientific Reports, 6*, 29308. doi:10.1038/srep29308

Woolf, T. B., Shepherd, G. M., & Greer, C. A. (1991). Serial reconstructions of granule cell spines in the mammalian olfactory bulb. *Synapse, 7*(3), 181-192.

Xiong, W., & Chen, W. R. (2002). Dynamic gating of spike propagation in the mitral cell lateral dendrites. *Neuron, 34*(1), 115-126.

Yu, X. M., Askalan, R., Keil, G. J., 2nd, & Salter, M. W. (1997). NMDA channel regulation by channel-associated protein tyrosine kinase Src. *Science, 275*(5300), 674-678.

Yu, X. M., & Salter, M. W. (1998). Gain control of NMDA-receptor currents by intracellular sodium. *Nature, 396*(6710), 469-474. doi:10.1038/24877

Zhang, L., Huang, Y., & Hu, B. (2016). Olfactory experiences dynamically regulate plasticity of dendritic spines in granule cells of Xenopus tadpoles in vivo. *Scientific Reports, 6*, 35009. doi:10.1038/srep35009

Zylbertal, A., Kahan, A., Ben-Shaul, Y., Yarom, Y., & Wagner, S. (2015). Prolonged Intracellular Na(+) Dynamics Govern Electrical Activity in Accessory Olfactory Bulb Mitral Cells. *PLoS Biology, 13*(12), e1002319. doi:10.1371/journal.pbio.1002319

Figure 1

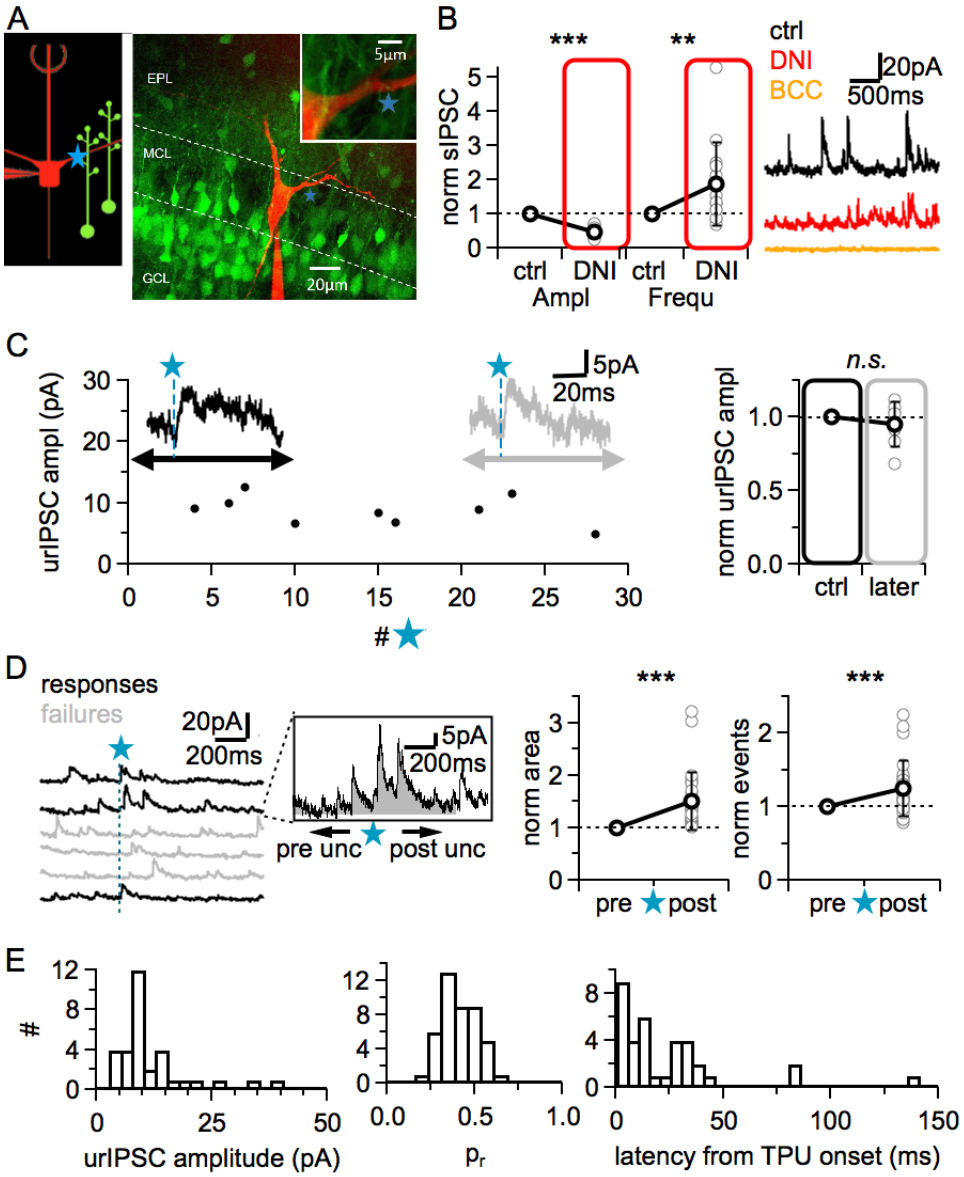

Figure 1. TPU-induced glutamatergic activation of GC spines triggers GABA release detected as urIPSCs in MCs.

(**A**) Experimental setting showing somatic whole cell voltage clamp recording from MC filled with Alexa 594 (red, 50 µM) and TPU of DNI-caged glutamate (DNI; blue star, 1 mM) at GC spines in VGAT-Venus rats (GCs green).

(**B**) Summary of effects of DNI (red) on spontaneous activity. Left: sIPSC amplitude and frequency (n = 14 MCs); Right: recordings from example experiment. sIPSCs are gone in the presence of bicuculline (BCC, orange, 50 µM).

(**C**) Left: Representative experiment showing individual urIPSC amplitudes over time. Inset: Averaged urIPSC in the first (black, n = 3 urIPSCs) and last ten minutes (grey, n = 3 urIPSCs). Right: Comparison of averaged normalized urIPSC amplitudes separated by 10 min interval (n = 7).

(D) Left: Example of consecutive uncaging traces showing urIPSC responses (black) and failures (grey). Inset: Integrals (grey) of 500 ms time windows pre and post uncaging. Middle: Area (integrated activity) in pre and post uncaging integrals in experiments where triggered urIPSCs were detected (n = 27). Right: Comparison between the number of pre and post uncaging IPSC events in the same data set (n = 27).

(**E**) Properties of first triggered urIPSCs. Left: Distribution of urIPSC amplitudes (n = 32, V_m = +10 mV). Middle: Distribution of release probabilities of GABA after TPU (n = 44). Right: Distribution of urIPSC latencies from TPU onset (n = 36).

Levels of significance (also in other figures): n.s., not significant, *: P < 0.05, **: P < 0.01, ***: P < 0.001

Figure S1

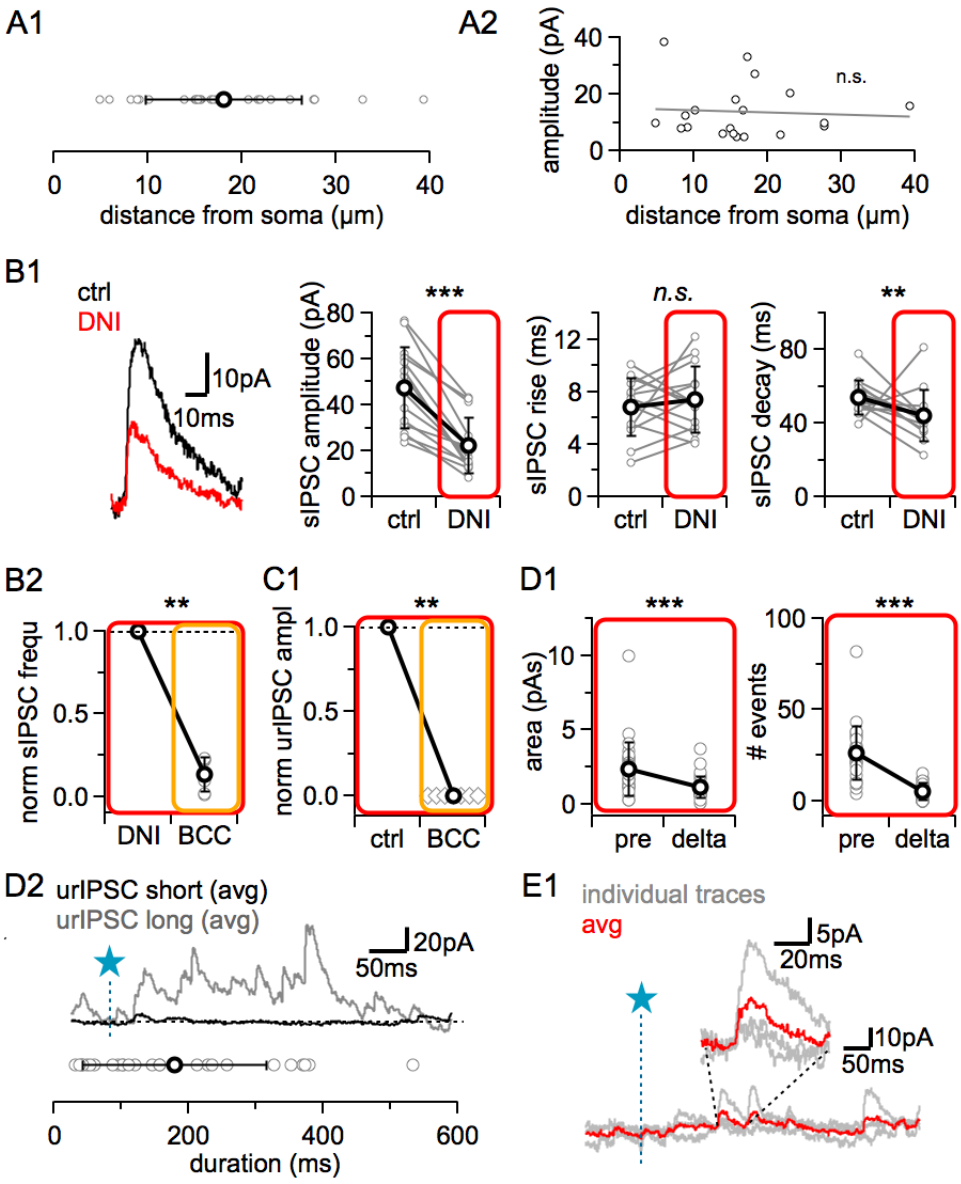

Figure S1. Secondary figure for Figure 1

Ad Fig. 1A: Location of uncaging sites. (**A1**) Cumulative data showing TPU distance from MC soma along lateral dendrites (n = 27). (**A2**) Correlation between urIPSC amplitudes and the site of TPU (n = 20).

Ad Fig. 1B: DNI significantly decreases sIPSC amplitude and leaves sIPSC kinetics unaffected. (**B1**) Representative events and summary plots showing the comparison of sIPSC parameters (amplitude, rise time, decay time, area) between control and in the presence of DNI (red, n = 14). (**B2**) Normalized frequency showing the effect of bicuculline (orange) on control (DNI) sIPSC activity (n = 6).

Ad Fig. 1C: (**C1**) The urIPSC is mediated by $GABA_A$ receptors. Normalized urIPSC amplitudes; signals are gone in the presence of bicuculline (n = 7)

Ad Fig. 1D: (**D1**) Absolute changes in area (integrated activity) and event numbers between ‚pre' interval and ‚post' interval (delta = ‚post' – ‚pre'). (**D2**) Quantification of extent of late/asynchronous activity: Duration of urIPSC barrages after TPU (n = 26); inset: examples for short average urIPSC (black) and long-lasting average urIPSC barrage (grey).

Ad Fig. 1E: (**E1**) Latency: Example of one of the three late first urIPSC recordings (> 50 ms). Representative traces with magnifying inset showing late triggered urIPSCs (individual traces: grey, average: red)

Figure 2

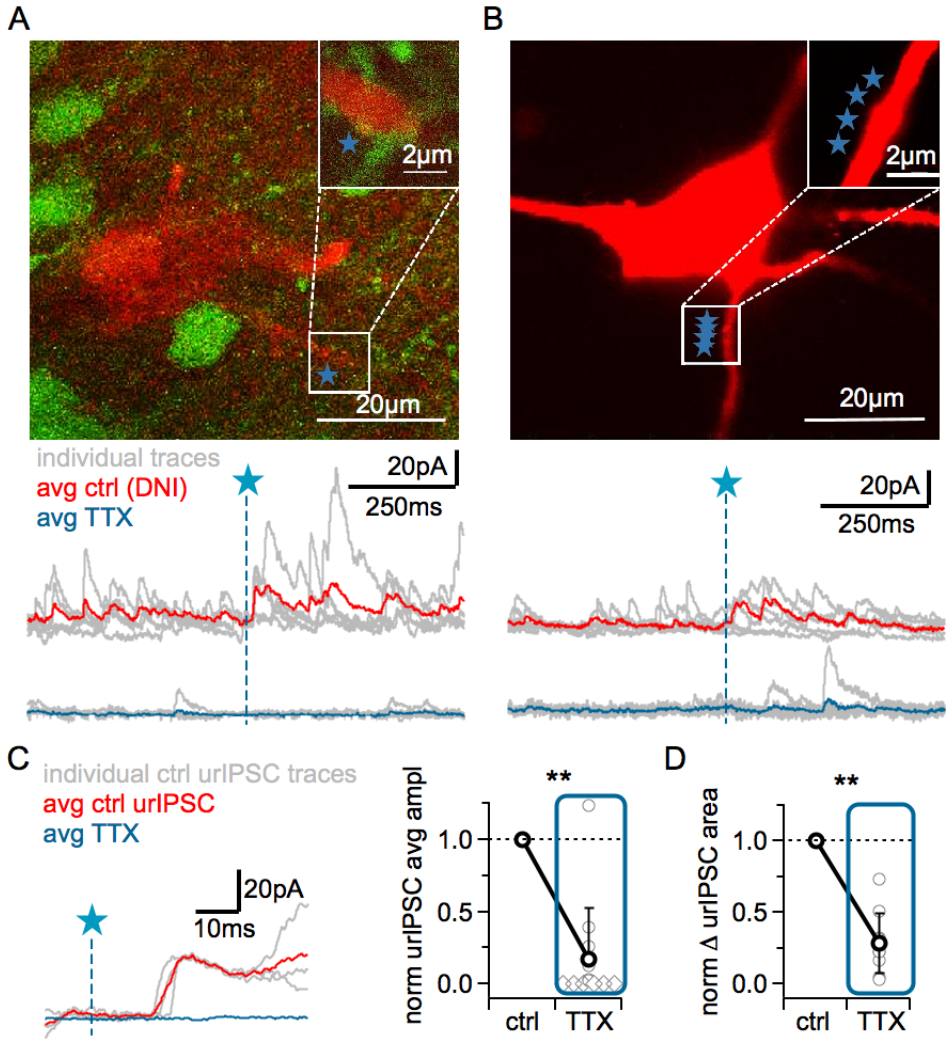

Figure 2. The urIPSC is reduced by Na_v blockade (TTX, 500nM).
(**A, B**) Representative experiments showing a patch-clamped mitral cell (Alexa594 50 µM, red), the uncaging site(s) along a lateral dendrite (blue star) and below the corresponding uncaging traces with individual traces shown in grey, average control traces in red and average TTX traces indicated in blue (A: VGAT-Venus rat, B: Wistar rat).
(**C**) Left: Magnified illustration of traces in A (for control individual traces with urIPSC responses and their average, for TTX only average, color coding as above). Right: Cumulative normalized data showing the strong reduction of urIPSC amplitude during Na_v blockade with TTX (n = 12). Diamonds indicate the experiments with no detectable response in the presence of the drug.
(**D**) Comparison of normalized delta IPSC area between control and in the presence of TTX (see Methods, n = 10).

Figure S2

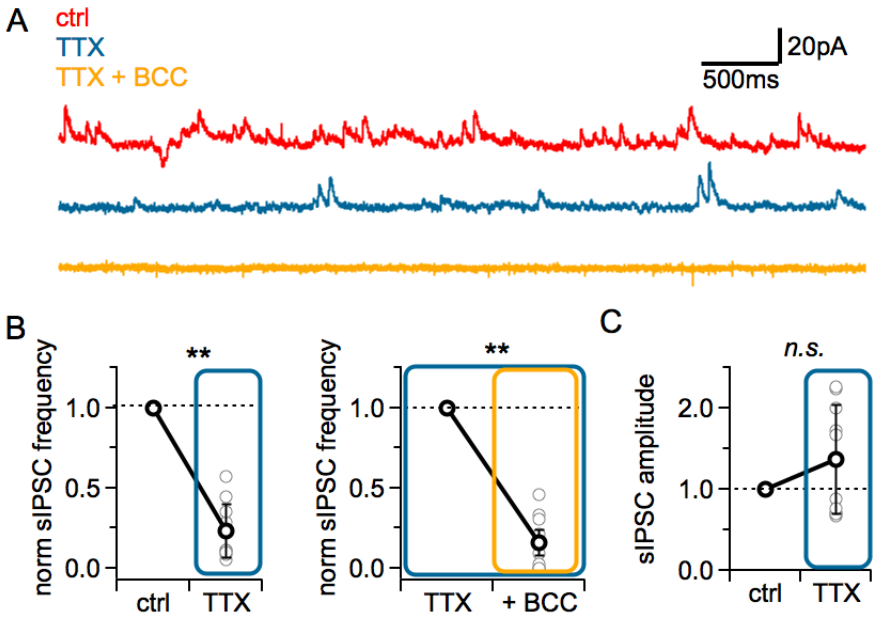

Figure S2: Secondary figure for Figure 2

Sodium channel blockade by TTX strongly attenuates spontaneous IPSC activity.

(**A**) Representative example of sIPSC traces in control (red), in the presence of TTX (blue) and additional application of bicuculline (orange).

(**B**) sIPSC frequency comparison beween control and additional presence of TTX (left, n = 10), between TTX and extra bicuculline added (+BCC, n = 10).

(**C**) Cumulative plot of normalized amplitudes illustrating the lack of an effect of Na_v blockade on spontaneous IPSC amplitudes (n = 9).

Figure 3

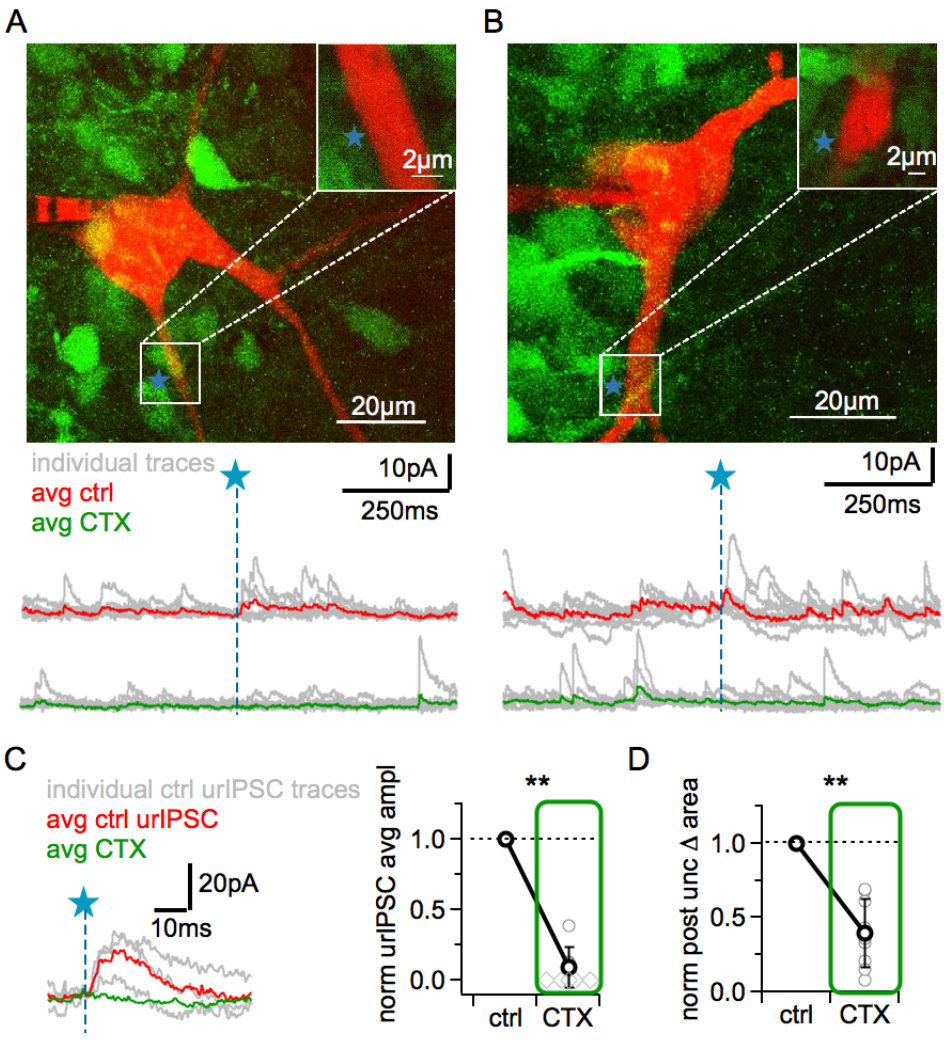

Figure 3.
Blockade of high voltage activated Ca^{2+} channels by ω-conotoxin MVIIC (CTX, 1 µM) causes a prominent reduction of urIPSC amplitudes.
(**A, B**) Two representative experiments in brain slices from VGAT-Venus rat with the corresponding MC (red), the site of TPU (blue star) and the uncaging traces according to the condition (individual traces : grey, average control: red, average CTX: green).
(**C**) Left: Magnified illustration of traces in B (for control individual traces with urIPSC responses and their average, for CTX only average, color coding as above). Right: Summary of effects of CTX on average normalized urIPSC amplitude (n = 8). Diamonds indicate the experiments with no detectable response in the presence of the drug.
(**D**) Comparison of delta urIPSC areas normalized to control versus in the presence of CTX (n = 9).

Figure S3

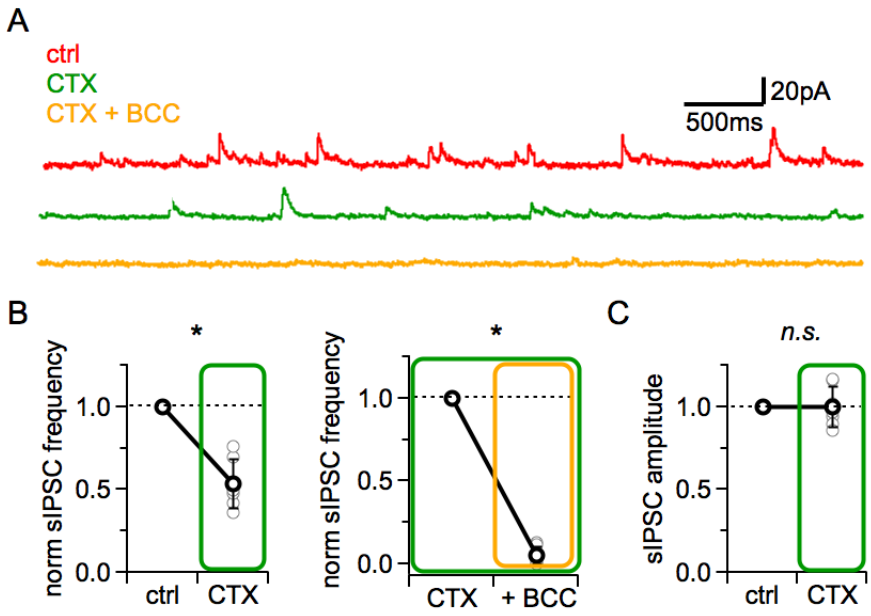

1016

1017

1018

1019 **Figure S3**. **Secondary figure for Figure 3**

1020 Spontaneous IPSC activity is lowered in the presence of CTX.

1021 (**A**) Example traces showing the decreasing effect of CTX (green) and bicuculline application (BCC,
1022 orange) on sIPSCs.

1023 (**B**) Normalized summary plots of the inhibitory effect of CTX (n = 7) and additional bicuculline (+
1024 BCC, n = 7) on sIPSC frequency.

1025 (**C**) Cumulative plot of normalized amplitudes showing no effect of CTX on sIPSC amplitudes (n = 7).

Figure 4

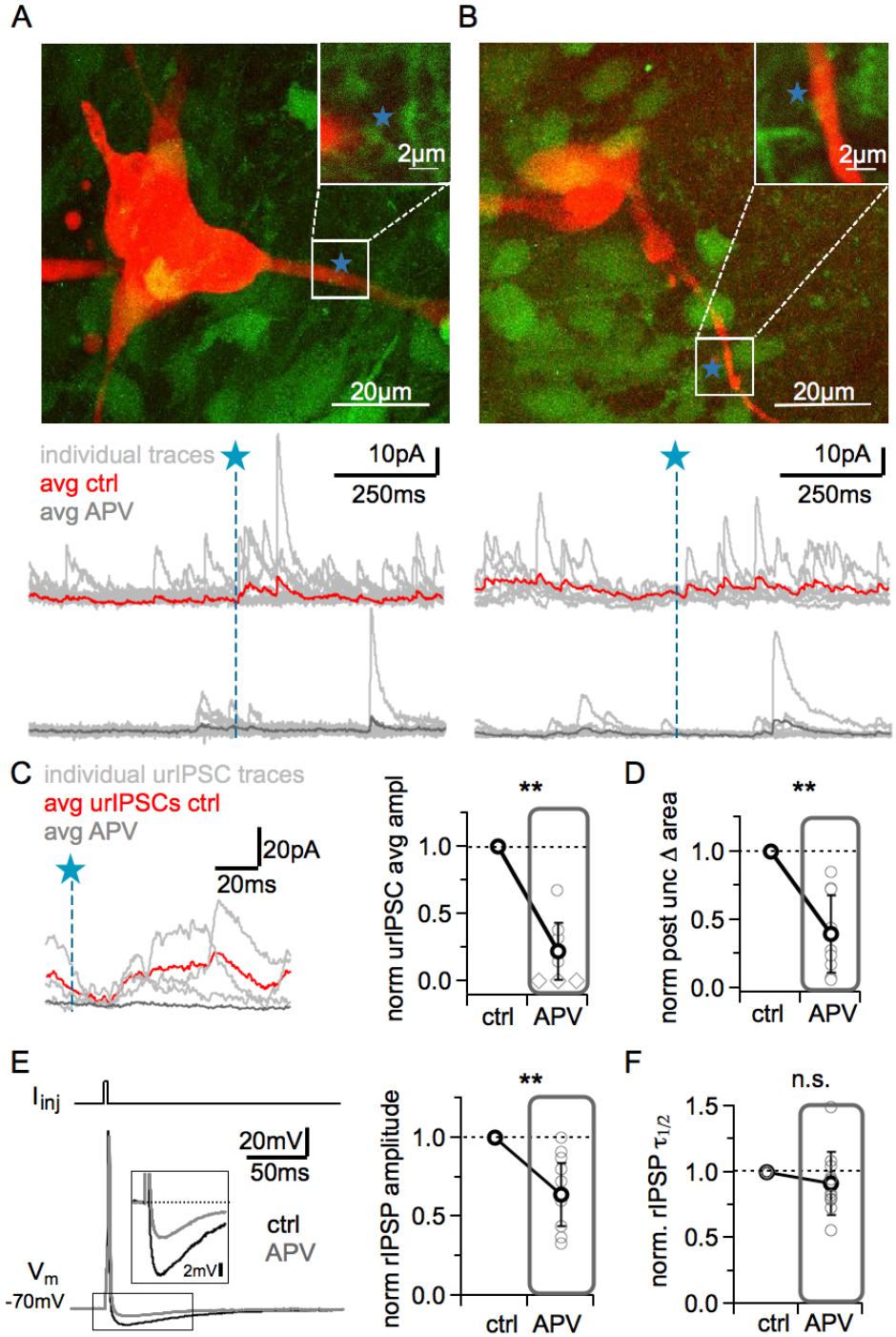

Figure 4. NMDAR blockade with D-APV (25 µM) results in a strong reduction of urIPSC amplitudes and also reduces rIPSPs following mitral cell APs.

(**A, B**) Shown are two representative uncaging experiments with the corresponding MC (red), the site of TPU (blue star) and the uncaging traces according to the condition (individual traces : grey, average control: red, average APV: dark grey; VGAT-Venus rat).

(**C**) Left: Magnified illustration of traces in A (for control individual traces with urIPSC responses and their average, for APV only average, color coding as above). Right: Summary of effects of APV on average normalized urIPSC amplitude (n = 10). Diamonds indicate the experiments with no detectable response in the presence of the drug.

(**D**) Comparison of delta urIPSC integrals between control versus in the presence of APV (n = 10).

(**E**) Left: Representative example of mitral cell AP evoked by somatic current injection in control conditions (black trace) and in the presence of APV (grey trace). Inset: Magnified recurrent IPSPs. Right: Summary of effects of APV on average normalized rIPSP amplitude (n = 11 MCs).

(**F**) Summary of effects of APV on normalized rIPSP half durations $\tau_{1/2}$ (n = 11).

Figure S4

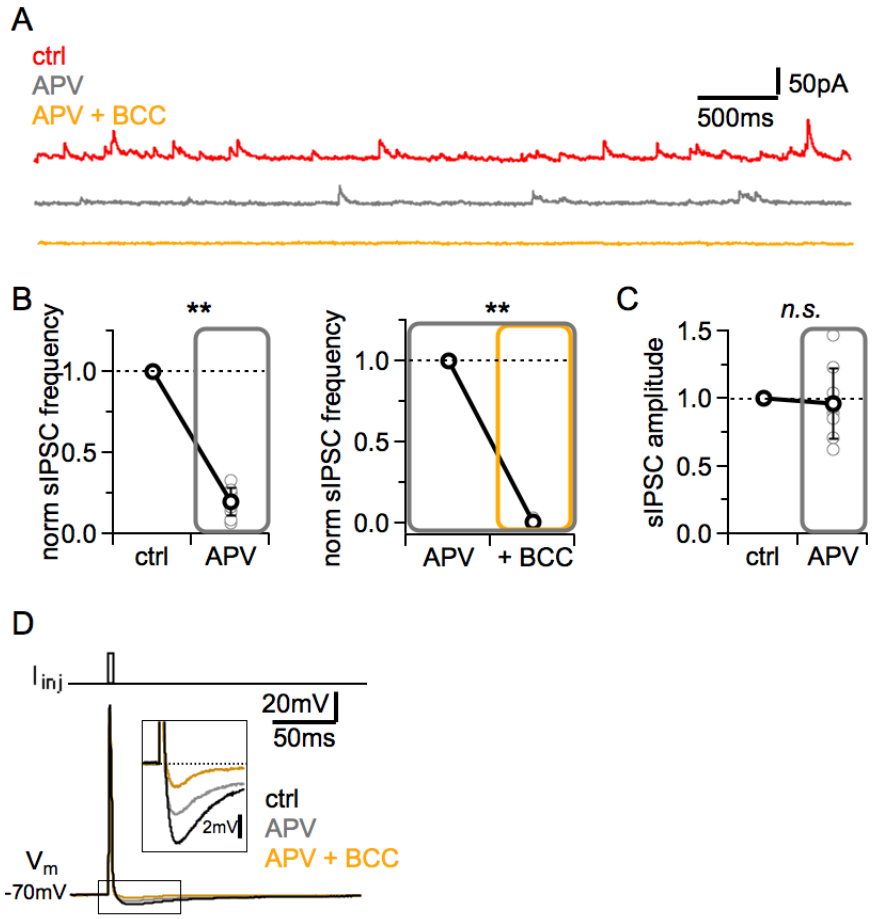

1041

1042

1043 **Figure S4**. **Secondary figure for Figure 4**

1044 NMDAR blockade by APV strongly depresses spontaneous IPSC activity.

1045 (**A**) Representative example of sIPSC traces in control (red), in the presence of D-APV (25
1046 µM, dark grey) and additional application of bicuculline (+BCC, orange).

1047 (**B**) sIPSC frequency comparison beween control and additional presence of D-APV (left, n =
1048 9), between D-APV and extra bicuculline added (n = 8).

1049 (**C**) Cumulative plot of normalized sIPSC amplitudes illustrating the effect of NMDAR
1050 blockade on spontaneous activity (n = 9).

1051 (**D**) Representative example of additional effect of $GABA_A$ receptor blockade with BCC on
1052 rIPSP in the presence of APV (after 25 min of wash-in).

Figure 5

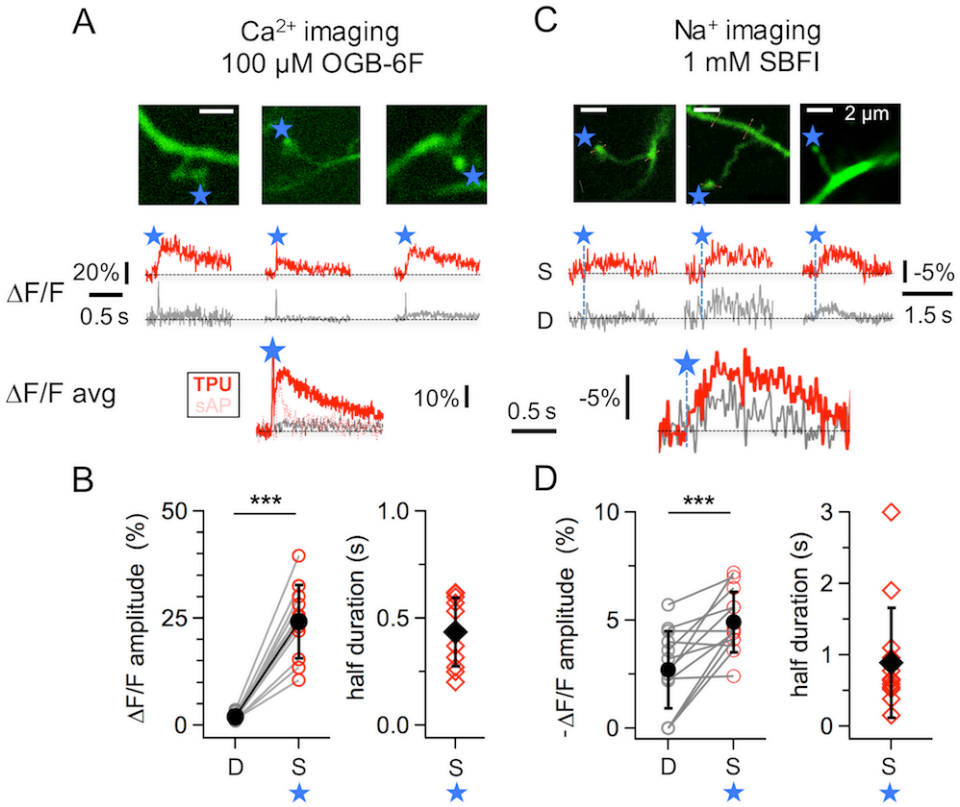

1053

1054

1055 **Figure 5**.

1056 Imaging of TPU-evoked Ca^{2+} or Na^{+} entry into GC spines with low exogenous buffering (100
1057 µM OGB-6F or 1 mM SBFI) reveals sluggish decay of $\Delta[Ca^{2+}]$ and plateau in $\Delta[Na^{+}]$.
1058 (**A, C**) Top: Representative examples of individual spines. Blue stars denote uncaging
1059 locations. Middle: Respective averaged fluorescence transients $(\Delta F/F)_{TPU}$ within the above
1060 spines (S, red) and the adjacent dendrite (D, black). Bottom: $(\Delta F/F)_{TPU}$ transients averaged
1061 across experiments (Ca^{2+} imaging: n = 11 spines, Na^{+} imaging: n = 13 spines) with the same
1062 time axis, spine response in red and dendrite response in grey. The dotted red trace in the Ca^{2+}
1063 imaging graph represents the averaged response to a backpropragating somatically evoked AP
1064 (n = 8).
1065 (**B, D**) Cumulative plots of $(\Delta F/F)_{TPU}$ amplitudes in dendrite and spine pairs and of half
1066 durations $\tau_{1/2}$ of $(\Delta F/F)_{TPU}$ within the spine heads (mostly not detectable in the dendrites).